NBS TECHNICAL NOTE

369

Interferometric Measurements of The Complex Dielectric Constant of Liquids

U.S. DEPARTMENT OF COMMERCE
National Bureau of Standards

NATIONAL BUREAU OF STANDARDS

The National Bureau of Standards[1] was established by an act of Congress March 3, 1901. Today, in addition to serving as the Nation's central measurement laboratory, the Bureau is a principal focal point in the Federal Government for assuring maximum application of the physical and engineering sciences to the advancement of technology in industry and commerce. To this end the Bureau conducts research and provides central national services in three broad program areas and provides central national services in a fourth. These are: (1) basic measurements and standards, (2) materials measurements and standards, (3) technological measurements and standards, and (4) transfer of technology.

The Bureau comprises the Institute for Basic Standards, the Institute for Materials Research, the Institute for Applied Technology, and the Center for Radiation Research.

THE INSTITUTE FOR BASIC STANDARDS provides the central basis within the United States of a complete and consistent system of physical measurement, coordinates that system with the measurement systems of other nations, and furnishes essential services leading to accurate and uniform physical measurements throughout the Nation's scientific community, industry, and commerce. The Institute consists of an Office of Standard Reference Data and a group of divisions organized by the following areas of science and engineering:

> Applied Mathematics—Electricity—Metrology—Mechanics—Heat—Atomic Physics—Cryogenics[2]—Radio Physics[2]—Radio Engineering[2]—Astrophysics[2]—Time and Frequency.[2]

THE INSTITUTE FOR MATERIALS RESEARCH conducts materials research leading to methods, standards of measurement, and data needed by industry, commerce, educational institutions, and government. The Institute also provides advisory and research services to other government agencies. The Institute consists of an Office of Standard Reference Materials and a group of divisions organized by the following areas of materials research:

> Analytical Chemistry—Polymers—Metallurgy — Inorganic Materials — Physical Chemistry.

THE INSTITUTE FOR APPLIED TECHNOLOGY provides for the creation of appropriate opportunities for the use and application of technology within the Federal Government and within the civilian sector of American industry. The primary functions of the Institute may be broadly classified as programs relating to technological measurements and standards and techniques for the transfer of technology. The Institute consists of a Clearinghouse for Scientific and Technical Information,[3] a Center for Computer Sciences and Technology, and a group of technical divisions and offices organized by the following fields of technology:

> Building Research—Electronic Instrumentation — Technical Analysis — Product Evaluation—Invention and Innovation— Weights and Measures — Engineering Standards—Vehicle Systems Research.

THE CENTER FOR RADIATION RESEARCH engages in research, measurement, and application of radiation to the solution of Bureau mission problems and the problems of other agencies and institutions. The Center for Radiation Research consists of the following divisions:

> Reactor Radiation—Linac Radiation—Applied Radiation—Nuclear Radiation.

NBS ◆ TECHNICAL NOTE 369

INTERFEROMETRIC MEASUREMENTS OF THE COMPLEX DIELECTRIC CONSTANT OF LIQUIDS

W. S. LOVELL AND L. M. THIEL

Radio Standards Physics Division
Institute for Basic Standards
National Bureau of Standards
Boulder, Colorado 80302

TABLE OF CONTENTS

Table of Contents - Continued

Interferometric Measurements of the
Complex Dielectric Constant of Liquids
I.   Errors in the "Perfect Square" Approximation

William S. Lovell

ABSTRACT

Errors arising from the use of a "perfect square"
approximation in treating free-space, interferometric meas-
urements of the complex dielectric constant $\epsilon* \equiv \epsilon' - i\epsilon''$ of
liquids are described. It is shown that such errors (1) are
generally positive, (2) often exceed values previously estimated
for the measurement technique as a whole, and (3) are not gen-
erally predictable without some prior knowledge of the dielectric
properties of the material being investigated. In addition,
these errors depend upon the dielectric thickness over which
data are incorporated into the calculations. Finally, an anomaly
in the calculations previously attributed to experimental error
is shown to arise from the "perfect square" approximation itself.
It is concluded that this approximation may at best provide initial
estimates for ϵ' and ϵ'' which may then be used in a more complete
mathematical treatment.

1. INTRODUCTION

The reflection of electromagnetic radiation at oblique incidence in free-space from an air-dielectric-metal configuration has been used to determine the complex dielectric constant $\epsilon^* \equiv \epsilon' - i\epsilon''$ of liquids at millimeter wavelengths.[1-4] The reflected power R as a function of the dielectric sheet thickness d yields a decaying interference pattern that has been described by the equation

$$R = \frac{\rho^2 - 2\rho \cos (2\beta d + \delta) e^{-2\alpha d} + e^{-4\alpha d}}{1 - 2\rho \cos (2\beta d - \delta) e^{-2\alpha d} + \rho^2 e^{-4\alpha d}} . \qquad (1)$$

This expression represents the modulus squared of the complex reflection coefficient for the configuration described. Reflection at the air-dielectric interface is described by the complex Fresnel reflection coefficient $\rho e^{i\delta}$ for the appropriate polarization, where ρ and δ are functions of ϵ^*, the angle of incidence θ_o, and the free-space wavelength λ_o of the incident radiation. The applications described[1-4] have been based on use of the coefficient for radiation whose electric vector lies perpendicular to the plane of incidence. At the dielectric-metal interface, reflection has been assumed to be perfect (reflection coefficient = -1) for a silver-plated metal. Propagation within the dielectric in a direction normal to the parallel air-dielectric and dielectric-metal interfaces is described by a complex propagation constant $k_d \cos \theta_d = \alpha + i\beta$, where θ_d is the angle of refraction.

Application of Eq. (1) to the determination of complex dielectric constants requires (1) demonstration that the equation describes experimental data with sufficient accuracy and (2) adequate mathematical treatment of the equation itself. Such a demonstration has not been given since complex dielectric constant measurements based on this reflection technique have consistently employed a mathematical approximation to Eq. (1). It is the purpose of this present paper to examine quantitatively the errors inherent in that approximation. For that purpose only, the assumption of a perfect reflection at the dielectric-metal interface will continue to be employed in

2

this paper.

To describe the approximation in question, in the limit $\delta = \pi$, Eq. (1) reduces to a "minimum envelope"

$$S = \frac{(\rho - e^{-n\alpha\lambda_d})^2}{(1 - \rho e^{-n\alpha\lambda_d})^2} \qquad (2)$$

for n a half-integer, and a "maximum envelope"

$$L = \frac{(\rho + e^{-n\alpha\lambda_d})^2}{(1 + \rho e^{-n\alpha\lambda_d})^2} \qquad (3)$$

for n an integer.[1] The index $n = \beta d/\pi$ designates successive minima and maxima in the reflection coefficient profile and $\lambda_d = 2\pi/\beta$ is the "wavelength" within the dielectric of the incident radiation. The use of Eqs. (2) and (3) to treat data presumably described by Eq. (1) we designate as the "perfect square" approximation.

At the same time, this paper is intended to serve as an introduction to subsequent papers of this series. The series as a whole is concerned with improvements in the interferometric technique for measuring the complex dielectric constant of liquids. Such improvements include a newly designed apparatus as well as extensions of the theory and mathematical techniques. In particular, consideration will be given to the true nature of the reflection at the dielectric-metal interface.

2. THE APPROXIMATION $\delta = \pi$

The validity of the perfect square approximation depends upon the degree to which $\delta \approx \pi$. For that reason, δ values have been calculated for a range of values of the complex dielectric constant using standard expressions for the complex Fresnel reflection coefficient. For radiation of free-space wavelength $\lambda_o = 2.143$ mm and angle of incidence $\theta_o = 35°$, results of these calculations are shown in the contour diagram of Fig. 1, where the phase shift δ is given in degrees. This figure was hand-drawn from computer-calculated δ values and does not show fine details in the

shape of the contour lines.

From the δ values indicated, it is clear that departures from the relation $\delta = \pi$ can be significant, particularly for high loss materials. The extent to which Eqs. (2) and (3) then fail to describe the extrema of Eq. (1) must then be determined. To illustrate this effect, we have selected the arbitrary values $\epsilon' = 2.50$ and $\epsilon'' = 0.40$, for which $\delta \approx 175°$, and calculated R vs d using Eq. (1), together with the corresponding "envelopes" defined by Eqs. (2) and (3). Resultant curves, which were both computer calculated and computer drawn, are shown in Fig. 2.

Even for the value $\pi - \delta \approx 5°$, these "envelope" curves fail to fit the extrema of Eq. (1) by amounts greater than the expected experimental error. It also seems worth noting that those points from Eq. (1) which most closely approach values defined by Eqs. (2) and (3) may occur at various points relative to the peak of each extremum. The question of precisely what power level should be fitted to Eqs. (2) and (3) in each case then becomes quite ambiguous.

For a different set of values of ϵ' and ϵ'', agreement between Eq. (1) and Eqs. (2) and (3) may be much better. For example, curves analogous to those of Fig. 2 using the values $\epsilon' = 2.62$ and $\epsilon'' = 0.28$, for which $\delta \approx 178°$, are shown in Fig. 3. In this case, the envelope curves are tangent to the extrema of Eq. (1) to a much better approximation.

However, a comparison of Figs. 2 and 3 shows that the range of dielectric thickness over which data points are selected introduces an additional variable in the use of the perfect square approximation. In Fig. 2, the envelope curves come closest to the extrema of Eq. (1) at small d values and then deviate as d increases, while in Fig. 3 the opposite behavior is found. Without prior knowledge of the complex dielectric constant being measured, one cannot then specify the range in dielectric thickness from which data points would yield the most accurate determination.

If we also consider that range of ϵ' and ϵ'' values in Fig. 1 for which measurements using the perfect square approximation might be carried out, the corresponding range in δ values suggests that the

4

resultant errors may be less than or much greater than those of the examples described. An adequate description of such errors then requires explicit calculation, both with respect to a range of ϵ' and ϵ'' and a range in d over which extremum valued are employed.

3. THE DETERMINATION OF ϵ' AND ϵ''

Determinations of ϵ' and ϵ'' using the perfect square approximation require values for the dielectric thickness increments Δd between successive maxima or minima ($\Delta d \approx \lambda_d/2$), together with the maximum and minimum power levels. In order to separate effects of the perfect square approximation from experimental errors, we have calculated such quantities directly from Eq. (1) for a series of values of ϵ' and ϵ''. For this purpose, an iteration technique known as the Method of False Position was employed (Appendix).

In practice, several of the minima of a given experimental curve are not used in subsequent calculations because their amplitudes are too small to be measured accurately. Which minima are deleted depends upon the complex dielectric constant of the material being investigated. This practice introduces an additional experimental variable separate from the perfect square approximation.

In analyzing this approximation mathematically, it would not be feasible to guess which minima would be deleted in practice. In order to treat this approximation more as it has been applied, however, we have arbitrarily deleted the lowest minimum from each calculation. It will be shown later that deleting such minima, whether in theory or practice, constitutes an additional source of systematic error when $\delta \neq \pi$.

The remaining amplitudes $S^{1/2}$ and $L^{1/2}$ and corresponding dielectric thicknesses d_n, obtained by iteration, were then treated using the same technique previously applied to experimental data.[2] However, initial values for the quantity $\alpha \lambda_d$ (used in calculating ρ^2) were not estimated but were calculated explicitly from the ϵ' and ϵ'' values used in each case. Values for ρ^2 were obtained from such $\alpha \lambda_d$ values, rather than directly, in order to duplicate the technique as previously employed. Resultant ρ values, together with the calculated $S^{1/2}$ and $L^{1/2}$ values, were then employed in Eqs. (2) and (3), rewritten in the form[2]

5

$$\exp(-n\alpha\lambda_d) = (\rho - S^{1/2})/(1 - \rho S^{1/2}) \tag{4}$$

and

$$\exp(-n\alpha\lambda_d) = (L^{1/2} - \rho)/(1 - \rho L^{1/2}), \tag{5}$$

care being taken to insure that the $S^{1/2}$ values had the correct sign.[1]
Resultant quantities $-\ln[\exp(-n\alpha\lambda_d)]$ vs n were then fitted by a straight line
of slope $\alpha\lambda_d$ using least squares.

The slopes $\alpha\lambda_d$ so derived differ from the exact $\alpha\lambda_d$ values previously
calculated by virtue of the perfect square approximation. Similarly, appli-
cation of these derived $\alpha\lambda_d$ values and calculated λ_d values in the equations

$$\epsilon'_{calc} = \left(\frac{\lambda_o}{\lambda_d}\right)^2 \left[1 - \left(\frac{\alpha\lambda_d}{2\pi}\right)^2\right] + \sin^2\theta_o \tag{6}$$

and

$$\epsilon''_{calc} = \left(\frac{\lambda_o}{\lambda_d}\right)^2 \frac{\alpha\lambda_d}{\pi} \tag{7}$$

leads to complex dielectric constant values different from the ϵ' and ϵ''
values used as input in each case. Differences between the input ϵ' and ϵ''
and output ϵ'_{calc} and ϵ''_{calc} values were then expressed as percentage errors
$\Delta\epsilon'$ and $\Delta\epsilon''$.

4. NONLINEARITIES IN $-\ln[\exp(-n\alpha\lambda_d)]$ vs n

In experimental applications of the perfect square approximation,
systematic departures from the straight line $-\ln[\exp(-n\alpha\lambda_d)] = n\alpha\lambda_d$ vs n
are found[5] such that points corresponding to the maxima lay above the line
while those for minima lay below the line. While this behavior was attrib-
uted[5] to experimental error, we have found similar departures in entirely
theoretical calculations. Calculated curves which illustrate this behavior
for the values $\epsilon' = 2.6$ and $\epsilon'' = 0.2$, 0.4, and 0.6 are shown in Fig. 4.

In the experimental case,[5] it was found that departures from the mean line were most pronounced for low loss materials, disappearing as the loss increases. In Fig. 4, it can be seen that the opposite behavior is found in a theoretical calculation. In spite of this difference, however, we suggest that the origin of this behavior may be the same in both cases.

In order for these systematic departures to be observed experimentally, it is necessary that (1) measurement errors must be smaller than the departure in question and (2) both minima and maxima must be included in these calculations in order that oscillation about a mean line can be established. In practice, both of these conditions preclude observation of these departures in measurements on higher loss materials.

At the same time, it is true both experimentally[5] and theoretically that deletion of minimum points from the calculations leads to systematic, positive errors in $\alpha \lambda_d$, since the slope of the mean line is thereby increased. It should also be noted, however, that this practice also leads to systematic, positive errors in λ_d.

It has been shown[6] earlier that wavelengths determined from spacings between maxima are consistently long, while those from minima are consistently short. Deletion of minimum points will then yield net positive errors in λ_d. This type of error differs from that previously described in that it decreases with increasing n. In Fig. 4, and particularly on the curve for $\epsilon'' = 0.6$, it can be seen that departures from the straight line increase with increasing n. The effects of either of these errors would be minimized if equal numbers of maximum and minimum points were included in the calculations.

Examination of Eqs. (6) and (7) indicates that positive errors in both $\alpha \lambda_d$ and λ_d lead to negative errors in ϵ', while the resultant errors in ϵ'' cannot be predicted without knowledge of the relative magnitudes of the errors in $\alpha \lambda_d$ and λ_d. All of the errors discussed in this section, however, constitute second-order errors. Of primary interest are the errors arising from use of the perfect square approximation in the best possible manner.

5.   ERRORS IN THE PERFECT SQUARE APPROXIMATION

Percentage errors arising from the perfect square approximation were calculated for a range of values of ϵ' and ϵ''. In determining ϵ'_{calc} and ϵ''_{calc}, all of the extrema in the range $n = \frac{1}{2}$ to $n = 4, 6,$ or 8 except the lowest minimum in each case were employed. For each of these ranges in dielectric thickness, the corresponding percentage errors in ϵ' and ϵ'' are plotted as functions of ϵ'', for various values of ϵ', in Fig. 5. The ϵ' values shown were chosen such that $\Delta\epsilon'$ increasing through the value 1% and $\Delta\epsilon''$ increasing through 2% would be illustrated. The curves were drawn through points calculated at increments of 0.1 in ϵ''.

From the figure, errors in both ϵ' and ϵ'' are generally seen to be positive and to increase with decreasing ϵ' and increasing ϵ'', i.e., with increasing loss tangent ϵ''/ϵ'. For ϵ'' values less than about 0.6, both errors are less than 2%. For such materials, both errors are decreased by using a greater number of data points. For higher loss materials, however, the error decreases when fewer points are employed. In any case, the differences in error arising from using different numbers of data points are nearly as large as the errors themselves. For fixed numbers of data points, the errors $\Delta\epsilon'$ and $\Delta\epsilon''$ over a wider range of ϵ' and ϵ'' are also shown in the contour diagrams of Fig. 6.

6.   CONCLUSIONS

It has been the purpose of this paper to provide the background for a more complete mathematical treatment of the reflection and interference process by which the complex dielectric constant of liquids has been measured, as well as to demonstrate the need for such analysis. That such analysis is needed is concluded on the basis that the perfect square approximation provides an inadequate test of the equation by which the interference phenomenon has been described. The experimental demonstration of certain anomalies in the use of this approximation is in itself evidence that the approximation errors exceed the experimental errors. Having access to

computers, there seems to be no reason why the mathematical treatment of such measurements should stand as a limit to their accuracy.

For purposes of estimation, on the other hand, if one does not have access to a computer, the perfect square approximation does provide dielectric constant values to a limited degree of accuracy. By the procedures given in this paper, such estimates may be made more accurate. The errors calculated in this paper may in fact be employed as corrections to the dielectric constant values obtained using the perfect square approximation. At the same time, such estimates may be employed as initial values in an alternative iteration procedure that will be described in a subsequent publication.

APPENDIX: DETERMINATION OF THE LOCAL EXTREMA

The thicknesses d_n, $n = \frac{1}{2}$, 1, ..., at which the extrema of Eq. (1) occur, are determined from the expression

$$R'(d_n) = 0, \quad n = \tfrac{1}{2},\ 1,\ \ldots \tag{8}$$

Since Eq. (1) is a transcendental equation, the sequence of solutions, $\{d_n\}$, is evaluated numerically. The first approximation to a given d_n is found by scanning the positive d axis by increments of length $(b-a)$ where $b > a$. When $R'(a) R'(b) \leq 0$ there is at least one solution in the interval $[a, b]$. By choosing $[a, b]$ such that

$$(b - a) < \frac{\lambda_d}{4}\ , \tag{9}$$

it is possible to insure that only one solution is bounded by $[a, b]$. Once the first approximation is found, the method of False Position (Regula Falsi)[7, 8] is used to determine the final solution to any desired accuracy. Each local extremum is then given by the coordinates

$$(d_n,\ R(d_n))\ . \tag{10}$$

ACKNOWLEDGEMENT

The author wishes to thank Lynn M. Thiel for the programming, application of the iterating technique, and other valuable contributions to this work.

REFERENCES

1. W. E. Vaughan, K. Bergmann, and C. P. Smyth, J. Phys. Chem. <u>65</u>, 94 (1961).

2. W. E. Vaughan, W. S. Lovell, and C. P. Smyth, J. Chem. Phys. <u>36</u>, 535 (1962).

3. V. M. Rao, Can. J. Phys. <u>41</u>, 1679 (1963).

4. M. Schünzel and M. Stockhausen, Z. Angew. Phys. <u>21</u>, 508 (1966).

5. W. E. Vaughan, S. B. W. Roeder, and T. Provder, J. Chem. Phys. <u>39</u>, 701 (1963).

6. C. Pine, W. G. Zoellner, and J. H. Rohrbaugh, J. Opt. Soc. Am. <u>49</u>, 1202 (1959).

7. A. S. Householder, <u>Principles of Numerical Analysis</u> (McGraw-Hill Book Company, Inc., New York, 1953), pp. 121-122.

8. D. Booth, <u>Numerical Methods</u> (Butterworths Scientific Publications, London, England, 1957), pp. 148-149.
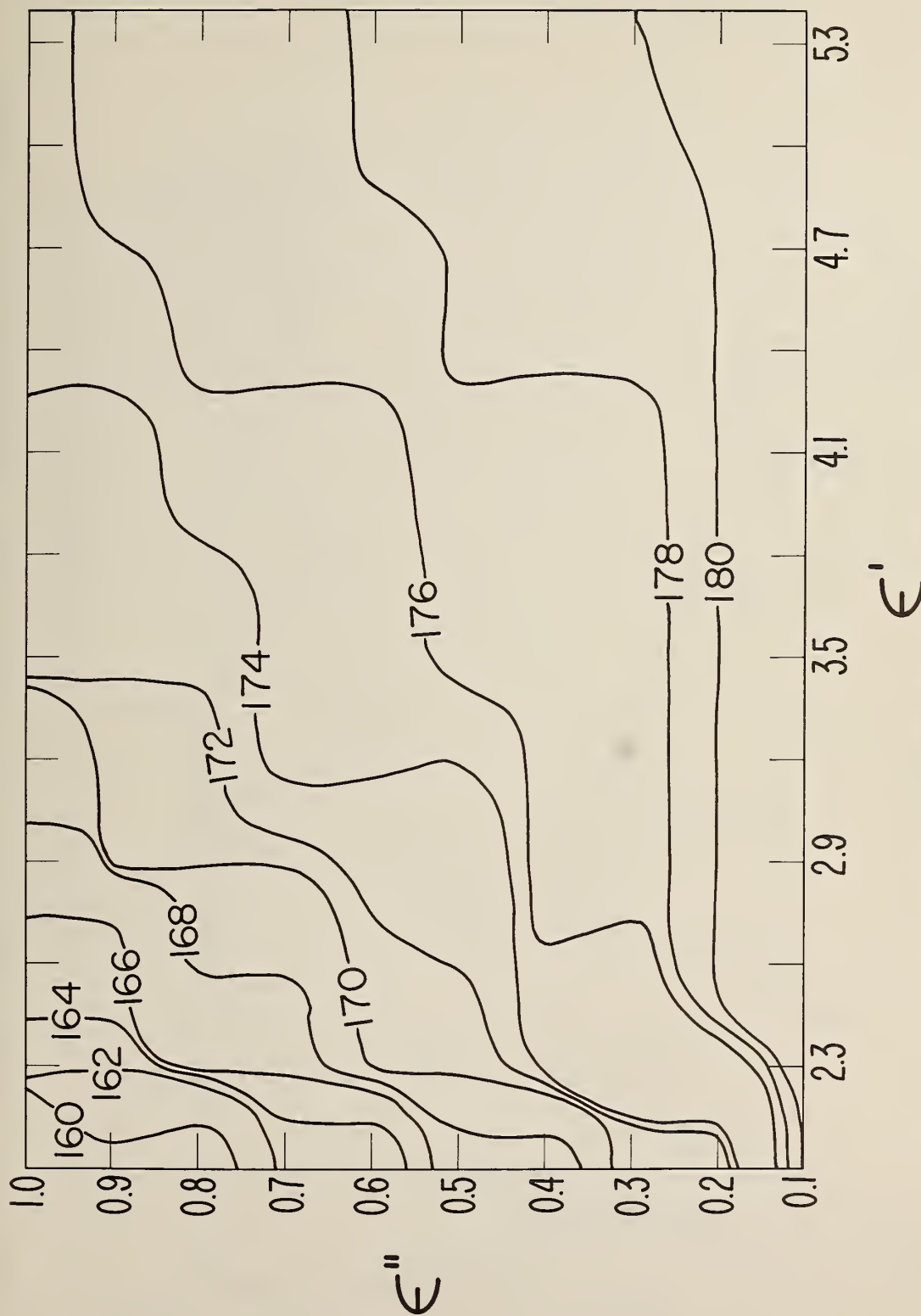
Figure 1: Contour diagram of the phase shift δ (in degrees) in the ϵ', ϵ" plane calculated from the complex Fresnel reflection coefficient for radiation whose electric vector lies perpendicular to the plane of incidence. Incident wavelength λ_o = 2.143 mm, angle of incidence = 35°.

13
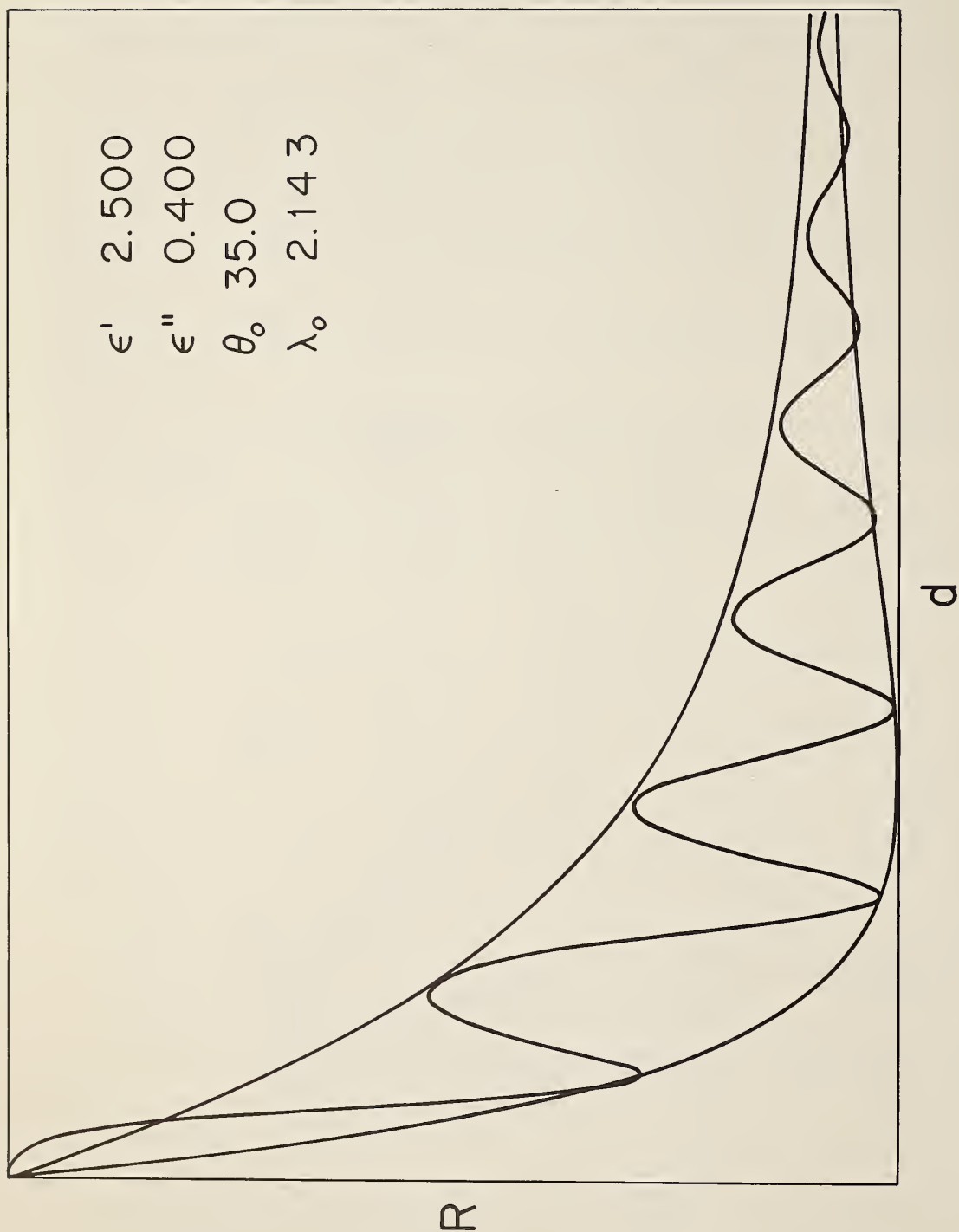
Figure 2: Reflected power R vs dielectric thickness d calculated from Eq. (1) (the interference curve) and Eqs. (2) and (3) (the minimum and maximum "envelopes"). $\epsilon' = 2.50$, $\epsilon'' = 0.40$.

ϵ' 2.500

ϵ'' 0.400

θ_o 35.0

λ_o 2.143

R

d

14

ϵ' 2.620
ϵ'' 0.280
$\theta_\circ$ 35.0
$\lambda_\circ$ 2.143

R

d
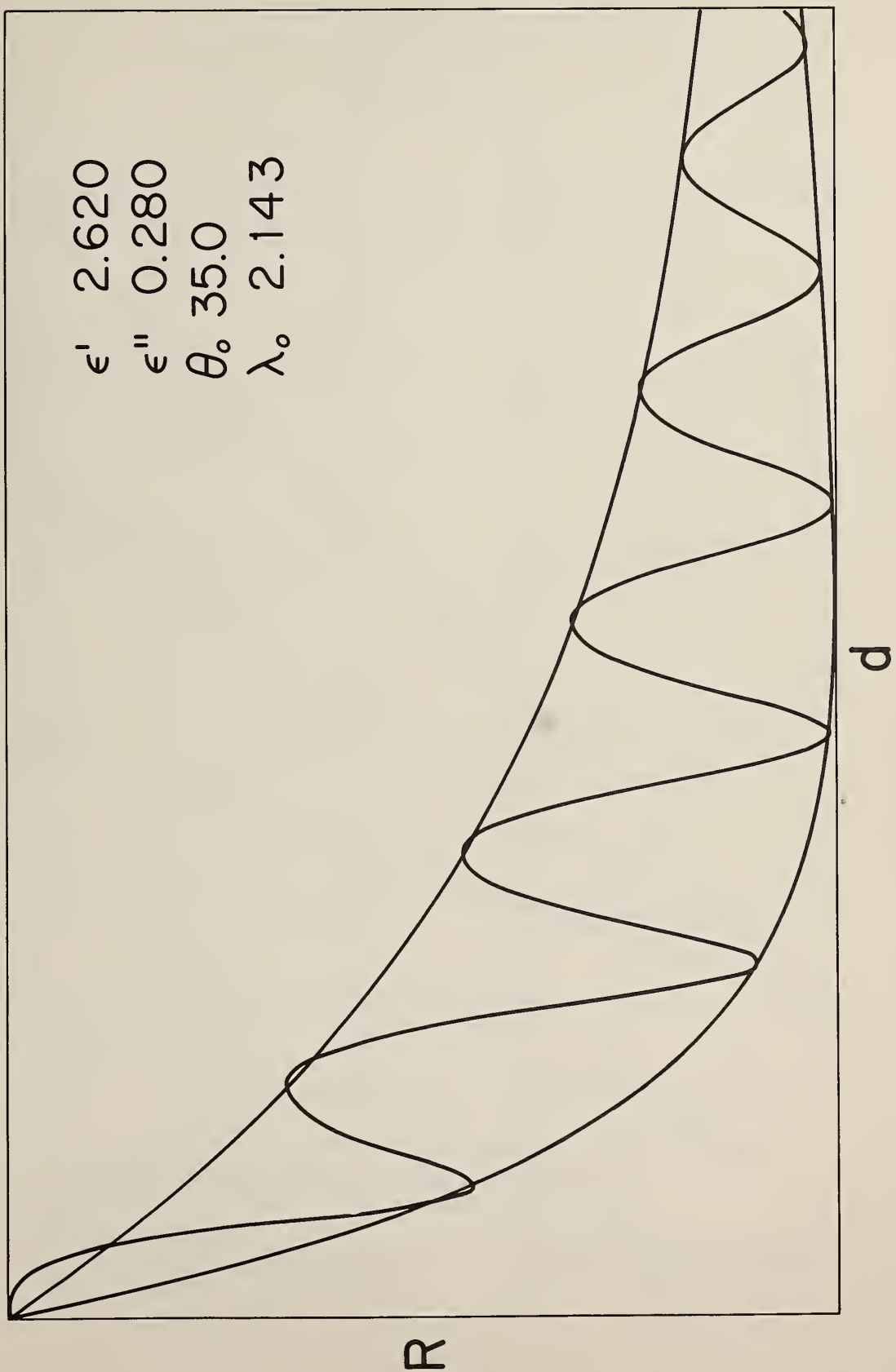
Figure 3: R vs d. $\epsilon' = 2.62$, $\epsilon'' = 0.28$.
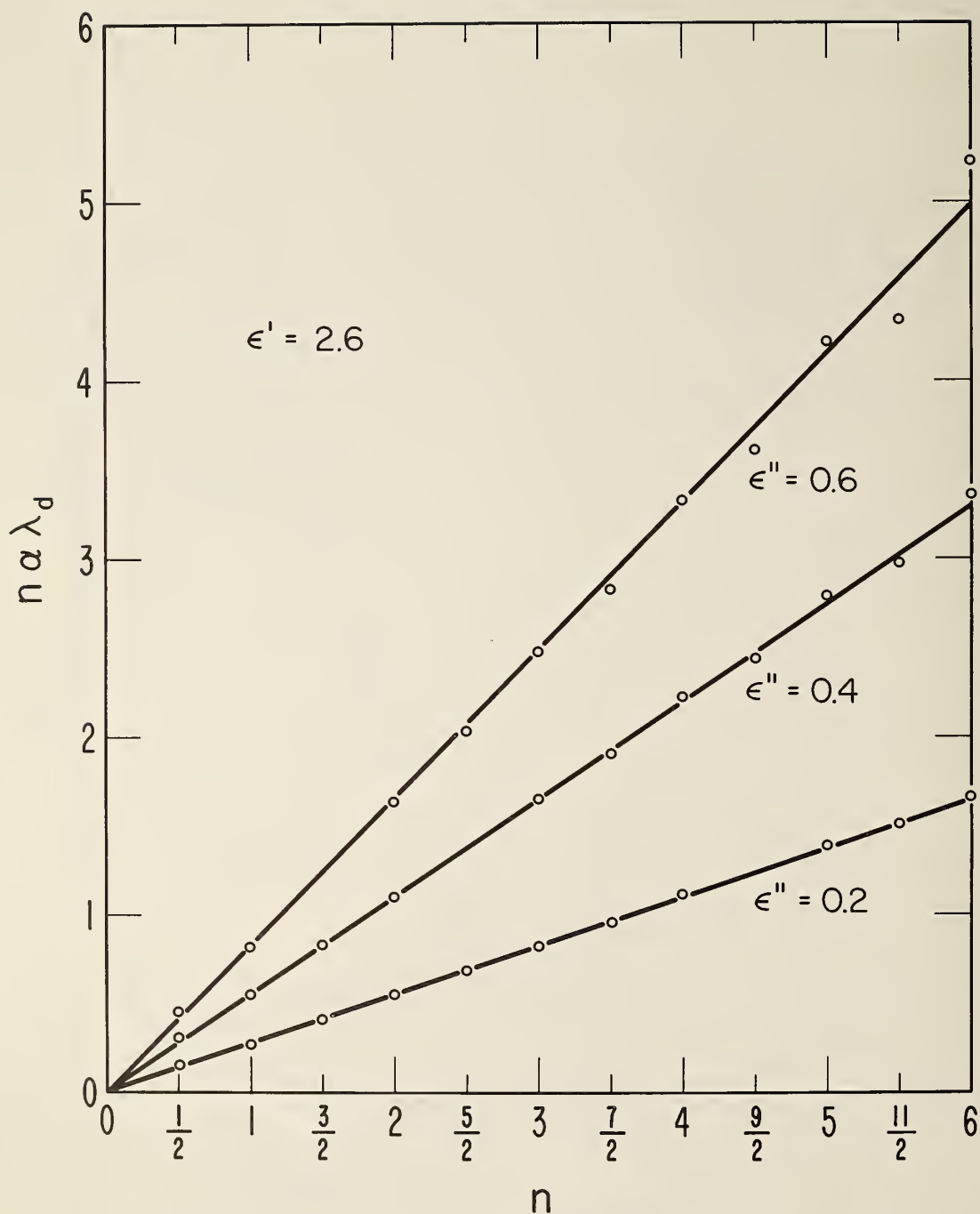
Figure 4: The least squares fit of the sequence of points
$\{ (-\ln[\exp(-n\alpha\lambda_d)] = n\alpha\lambda_d, n) \}$ from the perfect
square approximation. $\epsilon' = 2.6$; $\epsilon'' = 0.2, 0.4,$
0.6.

16
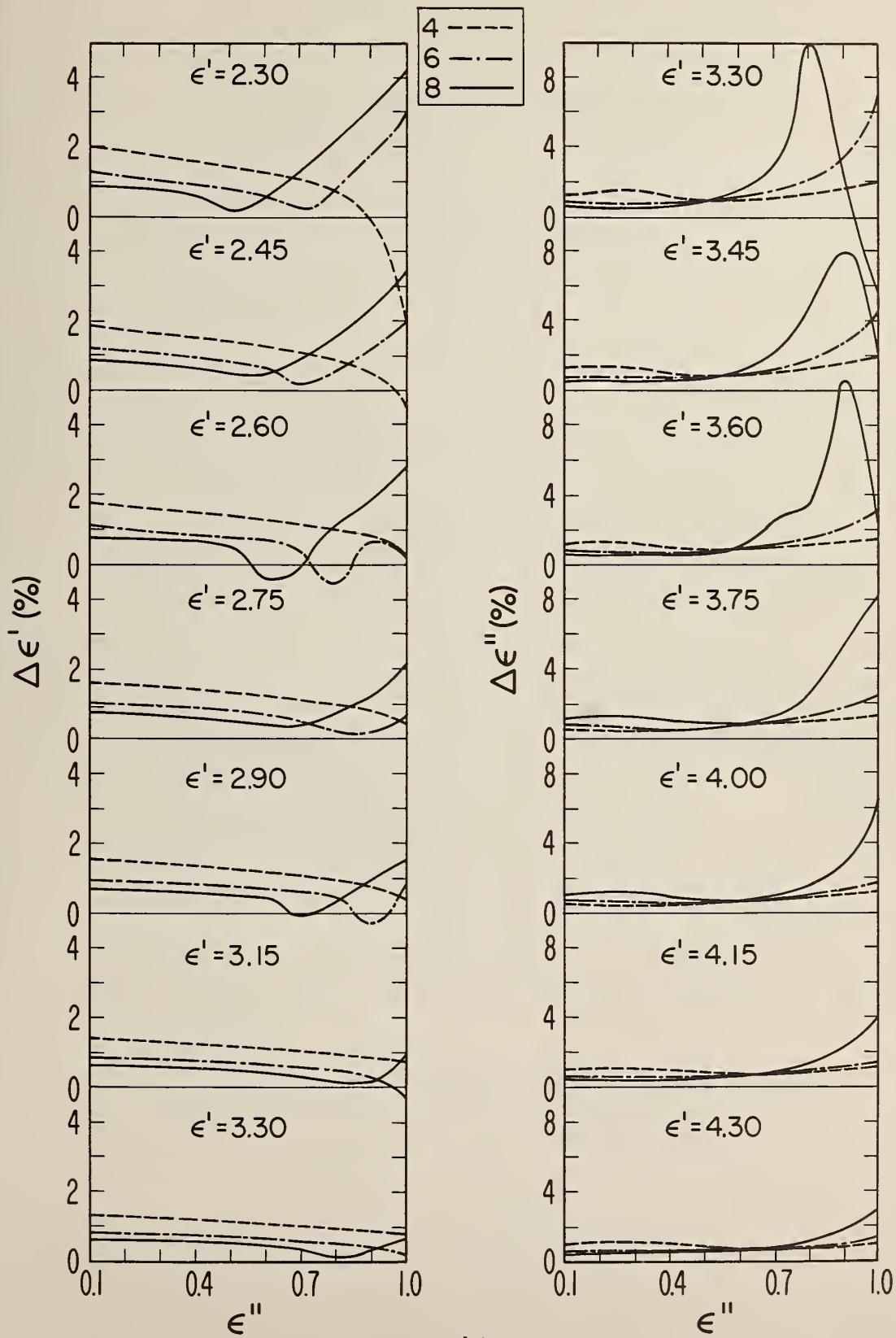
Figure 5: Calculated percentage errors $\Delta \epsilon'$ and $\Delta \epsilon''$ vs ϵ'' for seven values of ϵ' and three ranges of dielectric thickness $\frac{1}{2} \leq n \leq 4$; $\frac{1}{2} \leq n \leq 6$; and $\frac{1}{2} \leq n \leq 8$.
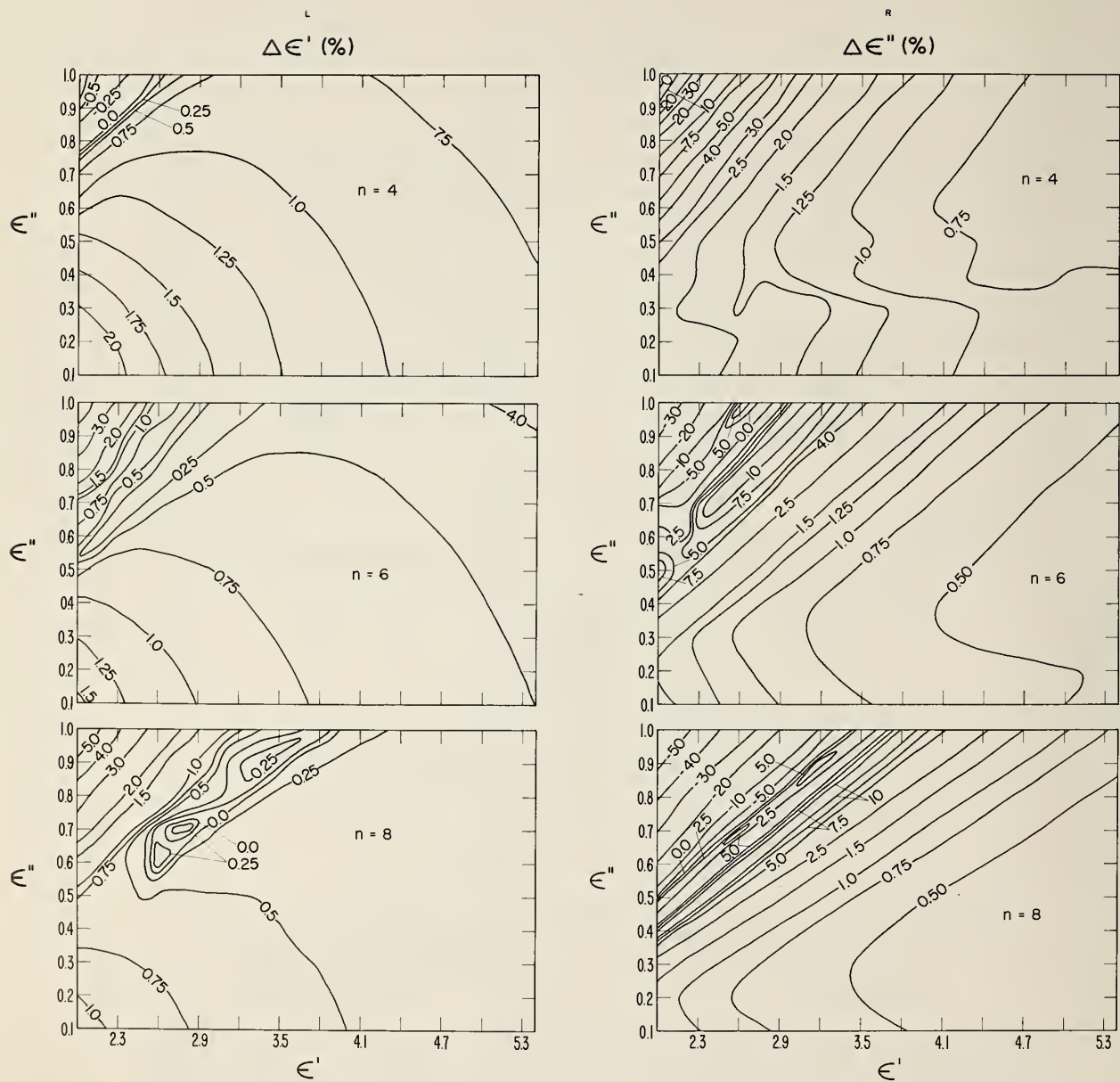
Figure 6: Contour diagram of the percentage errors Δ_ϵ' and Δ_ϵ'' in the ϵ', ϵ'' plane for three ranges of dielectric thickness.

18

Interferometric Measurements of the Complex
Dielectric Constant of Liquids
II. Experimental Apparatus

William S. Lovell

ABSTRACT

Design details of a free-space, millimeter-wave
interferometer are described. The apparatus radiates at oblique
incidence to an air-dielectric-metal configuration placed between
dissimilar horns. Errors arising from the quasi-optical nature
of this radiation are described, and quantitative data are pre-
sented which demonstrate techniques for minimizing such errors.
The techniques employed should have general applicability in
millimeter-wave measurements. For the particular instrument
described, the errors are shown to be of such magnitude that
experimental reflection coefficient profiles should conform to
an adequate theoretical description. A means for more accurate
and absolute measurements of the complex dielectric constant
of liquids is then provided.

1. INTRODUCTION

In the first paper[1] of this series (I), errors arising from the use of a mathematical approximation in treating free-space, interferometric measurements of the complex dielectric constant of liquids were described. It was concluded that such errors preclude an adequate test of the theory previously used to describe the reflection and interference process upon which such measurements are based.

The present paper describes an apparatus for measuring the complex dielectric constant of liquids at millimeter wavelengths by reflection and interference of electromagnetic radiation from an air-dielectric-metal configuration. The origins of energy losses in the system are also treated. Certain effects of a "quasi-optical" nature are also taken into account. An analysis of these effects is given as a basis for the particular equipment design to be described. This analysis includes quantitative data illustrating the manner in which errors arising from such effects are minimized. These data also show that for the instrument described, these effects will introduce negligible error.

This instrument then provides a means of testing the theory upon which its operation should be based, if the mathematical approximation mentioned earlier is not employed. Upon obtaining an adequate theoretical description of the reflection and interference process, together with the necessary mathematical tools, this instrument then provides a means for more accurate and absolute measurements of the complex dielectric constant.

2. APPARATUS

The largest component of the millimeter-wave interferometer consists of a goniometer device which establishes a vertical plane of incidence for the millimeter-wave radiation. A semicircular, 3/4-inch aluminum plate of 24-inch radius is mounted on a base having three adjustable legs for leveling purposes. To this plate are attached separate transmitting and

receiving arms which are loosely geared together and rotate about a common axis perpendicular to the plane of incidence. A diagram of this system is shown in Fig. 1.

With the introduction of a horizontal sample well, positioning of the transmitting arm then establishes the angle of incidence. Minor adjustment of the receiving arm then places the detector horn at the corresponding angle of reflection. The additional motional adjustments shown in the diagram are incorporated into the construction of the transmitting and receiving arms themselves.

On each arm, the millimeter-wave components are mounted on a slide operated by a precision lead screw which permits longitudinal motion through a range of 12 inches. The distance between each horn and the sample well is then adjustable over a range of approximately 10-40 cm.

At the same time, mounting of the millimeter-wave components on each slide is accomplished through use of circular precision bearings of 5-1/2 inch diameter at each end. The polarization angles relative to the plane of incidence for both the transmitting and receiving systems can then be rotated through 360 degrees. The bearings at the horn end of each system were preloaded such that runout with horn rotation was less than 0.0005 inch.

The sample cell, sketched in Fig. 2, was constructed primarily of aluminum and then zinc-plated after assembly. All joints connecting components within which the dielectric liquid would be placed were hard-soldered. Critical dimensions such as those of the piston, cylinder, and sample well were established by honing and replating followed by precise measurement at $68°$ F.

To describe the operation of this cell, the liquid dielectric is placed in a cylindrical reservoir within the cell through a fill port. A drain is provided at the bottom of the cell. Surrounding this reservoir is a water jacket connected through hoses to a temperature-controlled, circulating water bath. A thermometer leads into the water jacket through the top of the cell.

Above the reservoir, a reversible synchronous motor operating at 3 rpm drives a precision lead screw to force a cylindrical piston into the reservoir. Liquid is then forced through a small orifice into the sample well. The cross-sectional areas of the piston, reservoir, sample well, and fill pipe are such that the ratio of downward motion of the piston to increasing height of the liquid is 3.00008. The actual rate of increase of the liquid height is established as desired through setting the gear ratio between the motor and the lead screw, which has a pitch of 1 mm. The total range of travel of the piston is 9 cm. Allowing for a maximum dielectric thickness of 1 cm, the size of the reservoir is such that sample volumes in the range of 250-650 ml can be accommodated.

Concentric with the piston lead screw is a micrometer reading directly to 0.01 mm for determination of the piston height. Geared to the motor drive in a 3:1 ratio is a reversible shaft encoder registering 1000 counts per revolution to an accuracy of one part in 10^5. The output of the encoder leads to a 5-digit display module whose least count then represents 0.001 mm (1 micron) of dielectric thickness.

The cross section of the sample well may be described as a 10 cm square with semicircles of 10 cm diameter added to two opposite sides. The total depth of the well is one inch. At the bottom of the well is placed a silver-plated reflector approximately 1/4 inch thick having the same shape as the well. Beneath this reflector, the well is channeled to provide even flow of liquid onto the reflector from all sides. The reflector is easily removable for cleaning purposes, or for the insertion of additional spacers to adjust its height. To minimize vibration waves at the liquid surface, the sample cell, which itself weighs approximately 100 pounds when filled with water, is placed on a vibration-damping mount weighing 87 pounds.

The long dimension of the sample well (20 cm) lies parallel to a line through the thermometer well, piston axis, and fill port. In operation, the cell is placed so that the plane of incidence of the interferometer bisects the sample well through its long dimension. The fill port, piston drive,

and thermometer are then located in front of the area in which reflection takes place and are thus accessible during operation of the instrument.

Operation of the system as a whole may be described by reference to the block diagram shown in Fig. 3. Operating voltages for the klystron are provided by a regulated dc filament supply and a regulated reflector and beam supply, both operating from a line regulator. Attached to the klystron is a water jacket through which cooling water is circulated. A thermostat attached to the water jacket opens at temperatures above ambient to remove power from the klystron power supplies and prevent operation of the klystron without cooling water.

The klystron output, which is square-wave modulated at 1 kHz for detection purposes, leads to standard millimeter-wave components designed for the 90-140 GHz band. The power output of the klystron is approximately 120 mw. Through a ferrite isolator, the millimeter-wave radiation is led to a directional coupler where a -10 dB reference sample is taken off to a crystal detector. The main portion of the radiation passes through a dielectric attenuator and E/H tuner to a standard rectangular horn. For purposes to be described below, a dielectric lens is attached to this horn. The lensed horn is surrounded by microwave absorbing material.

On the receiving arm, the radiation reflected from the sample well enters another lensed horn of different design, also surrounded by microwave absorber, and passes through an E/H tuner and wavemeter to a crystal detector. The 1 kHz detected signal, together with the reference signal from the transmitting arm, is fed to a ratiometer. A voltage corresponding to the ratio of these signals, from which klystron noise has effectively been eliminated, is then fed to a digital voltmeter.

A frequency divider circuit operating from the line voltage is used to time the digital voltmeter readings. Such readings, together with the corresponding dielectric thicknesses as indicated by the display module, are fed to a digital recorder and constitute the experimental data for a given measurement of the complex dielectric constant. As a check on the

23

system, a chart recorder driven by a synchronous motor is connected in parallel with the digital voltmeter to provide a graphical record of the reflected power _vs_ dielectric thickness.

3. OPERATION

Application of this apparatus to a particular measurement requires determination of the angle of incidence θ_0 and wavelength λ_0 of the incident radiation. The former is determined geometrically, while the latter is obtained using the wavemeter. With such quantities known, there remain to be determined the reflected power levels and corresponding dielectric thicknesses to be used in the appropriate theoretical expressions.

However, the experimental data from the digital recorder must first be placed on the same scale as the theoretical expressions. It will be shown that the quantities necessary to define such scales cannot be measured with sufficient accuracy. The manner of actually determining these quantities will be described in a subsequent paper.

Dielectric Thickness Determination

In the course of a measurement, the dielectric thickness is increased by driving a piston into the sample reservoir which then forces liquid into the sample well by displacement. Initially, this liquid fills in the channeling and the space between the reflector and the walls of the well. At a certain position of the piston, depending on the volume of liquid in the reservoir, liquid then flows onto the reflector from all sides.

Because of surface tension, however, the liquid does not form a smooth layer above the reflector immediately, but only after a minimum volume of liquid has entered the well. The thickness of the dielectric layer first formed will depend upon the nature of the liquid and on the temperature.

24

The theory for the measurement process is based on the model of plane, parallel air-dielectric and dielectric-metal interfaces. Consequently, only those reflected power levels that are recorded after the smooth dielectric layer is formed constitute valid data. Evaluation of all subsequent dielectric thicknesses then requires determination of the actual thickness d_0 corresponding to the first such data point.

The quantity d_0 may be estimated by determining the thickness reading on the display module at which the liquid first begins to flow onto the reflector. Alternatively, the dielectric thickness might be calculated from measurement of the volume of liquid in the reservoir. However, such procedures cannot be carried out to the accuracy to which a dielectric thickness <u>difference</u> can be measured. As will be described in a subsequent paper, the accurate measurement of such a difference permits an accurate determination of d_0 to be made mathematically.

A source of error in determination of the dielectric thickness by measurement of the sample volume is evaporation. Of course, such evaporation must take place during the course of a dielectric constant measurement as well. Evaporation may be reduced by surrounding the sample cell with an air-tight enclosure and allowing the system to equilibrate before a measurement is begun.[2] To describe such evaporation as does occur, it has been assumed[2] that the dielectric thickness decreases linearly with time t. On that assumption, evaporation effects should be cancelled out if one averages two curves of the reflected power R <u>vs</u> thickness d, one taken with increasing d and the other with decreasing d.

Although such a procedure does double the number of experimental measurements that must be made, the assumptions upon which it is based seem reasonable. However, if one is to treat the equations describing the reflected power R <u>vs</u> d explicitly instead of approximately,[1] it becomes not only possible but necessary to incorporate that assumption of a linear evaporation rate into such equations.

25

Since the dielectric thickness as determined by the synchronous motor drive varies linearly with time, the evaporation rate may be described in reference to d rather than t. An evaporation constant κ in millimeters of liquid evaporated per millimeter of change in dielectric thickness as indicated by the display module may then be defined. This constant is measured using assumed dielectric thickness values d_a taken from the display module. Taking account of the initial thickness translation d_0, the dielectric thickness d may then be expressed as

$$d = (1 - \kappa) d_a + d_0, \tag{1}$$

where the values d_a are those given by the digital recorder. In practice, since measurements are taken at equal intervals in d_a, only the first and last of N values of d_a are recorded, and intermediate values are then calculated. Using preset switches incorporated into the display module, a final d_a value may be preselected and used to shut off power to the synchronous motor driving the liquid at the end of a measurement.

Power Level Determination

The assumption that a perfect reflection occurs at the dielectric-metal interface suggests the use of a reflection coefficient defined as[3] $R = |E_2/E_0|^2$, where E_0 and E_2 represent the amplitudes of the incident and reflected electric vectors, respectively, and $0 \leq R \leq 1$. The corresponding theoretical expression[1-4] for R, given as Eq. (1) in I, is also normalized since it reduces to unity for $d = 0$. The reduction of experimental data to this scale is accomplished by the correspondence[3,4] $R_0 \leftrightarrow 1$, where R_0 is the reflected power measured at zero dielectric thickness.

However, energy may be lost by another means even if the reflection is perfect. Some energy may not reach the receiving horn because of divergence in the transmitted beam. Ohmic losses in the waveguide, reflections, and scattering in the lenses may also reduce the power detected at the receiving

horn. All such actual energy losses may be described in terms of a trans-
mission coefficient T, where $0 < T < 1$, and the reflection coefficient may be
<u>redefined</u> as $R = T|E_2/E_0|^2$. For a perfect reflection at zero dielectric
thickness, the power R_0 would then be described as $R_0 = TR_M$, where R_M
is defined as the maximum power output of the transmitting system beyond
the attenuator. Using the correspondence $R_M \leftrightarrow 1$, R becomes normalized
and describes the total energy transfer to the receiving system, including
both transmission and reflection processes.

Application of this scale in such a manner would require determination
of R_M (or R_0 and T). Using the apparatus described by the block diagram in
Fig. 3, power measurements consist of voltages recorded from the digital
voltmeter. Even in a direct measurement of the received power, the actual
magnitude of such voltages would depend, among other things, upon the
attenuator setting and the efficiency of the crystal detector on the receiving
arm. For the purpose of eliminating klystron noise from the power measure-
ments, the apparatus includes an additional circuit consisting of the directional
coupler and a second crystal detector. The ratio of the power levels detected
in the two branches is then taken by the ratiometer, so that the attenuation and
crystal efficiency in the reference branch also affect the voltage levels actually
recorded.

The operation of the circuit as a whole then depends upon the relative
millimeter-wave power in the two branches, as determined by the attenuation
ratio between the attenuator and directional coupler; the relative detected
power as determined by the ratio of the crystal detector efficiencies; and the
final voltage reading as determined by the amplification factor of the ratio-
meter. In contrast to the actual energy losses described by T, these effects
represent apparent power changes, and their net effect could be adjusted to
any desired value for a given measurement of the complex dielectric constant.

For the purpose of relating the experimental record in such a measure-
ment, consisting of the set of N voltages $\{R_i \,|\, i = 1, \ldots, N\}$, to a theoretical
reflection coefficient, the effects described may be represented by a gain

factor G. The perfectly-reflected power at zero dielectric thickness would then be represented by $R_0 = GTR_M$, where R_0 now represents a voltage as indicated on the digital recorder. Determination of R_M in this case would require determination of R_0 and the product GT. Assuming a perfect reflection, R_0 could be measured using the configuration shown in Fig. 1, while GT could only be obtained by some disassembly of the millimeter-wave components.

Apart from the inconvenience of such a procedure, the value of the product GT so obtained would have to remain constant throughout reassembly and a subsequent dielectric constant measurement. Dependent as GT would be upon the attenuator setting, tuning of the detectors and E/H tuners, temperature variations in the detector sensitivities, and ratiometer gain, the assumption that GT would remain so constant could not reasonably be made. For that reason, a means is required for determining GT using the configuration shown in Figs. 1 and 3.

By virtue of the factor GT, the voltage R_0 and the values R_i obtained in a dielectric constant measurement would be described on an equivalent basis provided that perfect reflection occurs at the dry plate. In the theory for the reflection coefficient given in the following paper in this series, however, that reflection is assumed not to be perfect. On the other hand, in relating R_0 and R_i, the restriction to perfect reflections can be eliminated since the theoretical expression for the reflection coefficient $R(d)$ includes the case $R(0)$ for $d = 0$. Whether reflection at the dry plate is perfect or not, the voltage R_0 may be described as $R_0 = \Gamma_0 R(0)$, where we define $\Gamma_0 \equiv GTR_M$.

This formalism now places the experimental data R_i and the theoretical expressions $R(d)$ entirely on the same scale. The transformation required may be written as

$$R_i = \Gamma_0 R(d_i), \tag{2}$$

where d_i is the dielectric thickness corresponding to the voltage R_i, and R_0 represents the special case for $d = 0$. By making use of that special case, either GT or R_M could be determined if the other were known.

28

That step is not necessary, however, since the R_i values may be used for the same purpose. Since the factors G, T, and R_M are not themselves of intrinsic interest, all that is required is a value for the product Γ_0. As will be described in a subsequent paper of this series, the R_i values essentially provide a set of simultaneous equations from which Γ_0, as well as the d_0 and κ values described earlier, may be obtained incidentally in the course of obtaining the value of the complex dielectric constant.

4. INSTRUMENTAL ERRORS

The description given so far of the apparatus and its operation, together with the theory and mathematical procedures described in subsequent papers of this series, suffice to establish the manner in which complex dielectric constant data are obtained using this interferometric technique. However, the accuracy of such data will depend upon the degree to which several sources of error originating in the apparatus have been minimized. For the most part, these effects arise from the "quasi-optical" nature of the millimeter-wave radiation and lead to extraneous variations in received power as a measurement is made which cannot be described by a constant such as Γ_0. The remainder of this paper treats the origin of these effects in detail and outlines the manner in which their resultant errors may be reduced.

The fundamental requirement for accurate dielectric constant data is that the experimental record as taken from the digital recorder must incorporate no extraneous effects such that it cannot be described by the theory. As will be shown in more detail in a later paper, demonstration that the theory and experimental data are consistent is based upon a "goodness of fit" criterion. The complex dielectric constant data obtained are then subject only to random error, which can be treated statistically.

Standing Wave Effects

The presence of a standing wave pattern along the horn-cell-horn propagation axis has previously been noted.[2,3] This pattern arises from reflection of millimeter-wave radiation at each of the horn-air interfaces. In a dielectric constant measurement, introduction of the dielectric changes the optical distance between the horns. As a result, a sinusoidal variation in power of period $\lambda_0/2$ becomes superimposed on the measured reflection coefficient profile. Translation of the receiving horn by $\lambda_0/4$ to shift the standing wave pattern between successive measurements and averaging of the resultant curves has previsously been employed to eliminate this effect.[2,3]

The amplitude of the standing wave pattern may be reduced by tuning the klystron and adjustment of the E/H tuners on both arms.[2] In the present apparatus, this pattern is further reduced by surrounding the horns with microwave absorber, thus reducing the reflection of radiation from one horn back to the other. In addition, the lenses on each horn, attached for purposes to be described below, may act somewhat as impedance matching devices to reduce further the reflections at the horn-air interfaces. Through some combination of these effects, reflection coefficient profiles measured on this instrument at receiving horn positions separated by $\lambda_0/4$ have been found to be indistinguishable on an ordinary strip chart recorder. For this reason, complex dielectric constant data are then calculated from a single experimental record.

In the absence of dielectric, however, a standing wave pattern can still be detected, either by relative motion of the horns or by motion of the reflecting plate in the cell. The purpose of the latter procedure and the apparent absence of a standing wave pattern in the experimental record will be discussed below.

Diffraction Effects

The influence of "diffraction effects" on this measurement technique has previously been noted.[2-4] Diffraction occurs in any case in which the millimeter-wave radiation traverses an aperture sufficiently small in terms of wavelengths. Separate diffraction effects may be distinguished by reference to the aperture involved. In the present apparatus, the transmitting horn, receiving horn, and sample well comprise such apertures.

A certain diffraction pattern may then be said to exist in reference to the horn-well-horn axis. In a dielectric constant measurement, however, that pattern can only be seen by virtue of a change in the geometry of the system in the course of a measurement. Any constant difference in power arising from the diffraction pattern would be incorporated in the constant Γ_0. Such changes occur only at the sample well, through the introduction of dielectric; hence, it is in reference to that aperture that discernible diffraction effects must be described.

To describe the motions involved, it can be seen in Fig. 1 or in the exaggerated sketch shown in Fig. 4, that the transmitting and receiving horn axes cross at a single vertex. The propagation axis is colinear with both of those axes, so that maximum power is received, only when the reflecting plane in the cell is at a height corresponding to that vertex. If the reflecting plane is moved upward by a distance h, the point on the plane originally coinciding with the vertex moves a distance $h \sin \theta_0$ transversely and $h \cos \theta_0$ longitudinally with respect to each horn axis. The propagation axis then moves a distance $2h \sin \theta_0$ transverse to the receiving horn axis and decreases in length by $2h \cos \theta_0$. Both components of this motion are expected to affect the power level measured at the receiving horn.

For purposes of discussion, those components of motion may be treated separately in their relation to the diffraction pattern. Because of the relative size of the apertures involved, that pattern may be said to arise primarily from horn diffraction, i.e., the millimeter-wave radiation appears in a finite beam having a definite radiation pattern. Transverse motion of that beam may be described as a beam displacement, and will be discussed

31

in the following section. Longitudinal motions, for which the dimensions of the sample well may become relevant, may be treated more easily in terms of a diffraction effect.

In a dielectric constant measurement, the plane defined by the dielectric-metal interface is not moved and may be placed at the vertex of the horn axes. The air-dielectric interface necessarily moves, however, and in the manner shown in Fig. 4. That motion does not change the physical horn-reflector-horn distance, but it does change that optical distance. For a dielectric thickness d, longitudinal motion relative to the diffraction pattern results from the replacement of air by dielectric liquid over a distance $2d \cos \theta_0$. It is this same motion, of course, which leads to the super-position onto the reflection coefficient profile of any standing wave pattern present, as discussed in the previous section.

In order to examine the magnitude of any variations in power resulting from the diffraction effect, it must be separated from those interference effects which yield the desired reflection coefficient profile. This diffraction effect could be simulated by placing an equivalent aperture centrally on a line between facing transmitting and receiving horns and moving those horns symmetrically along their common axis. Such a procedure is inconvenient, however, and may be approximated by a series of measurements at fixed horn-horn distances in which the aperture is moved along the horn-horn axis. Using pyramidal horns of 1.8 × 2.2 cm aperture and an operating frequency of 110 GHz, results of such a set of measurements are shown in Fig. 5.

To obtain these curves, a circular aperture whose diameter is indicated under each set of curves in Fig. 5 was centered about the horn-horn axis and then drawn from one horn to the other by a synchronous motor. Simultaneously, the detected power at the receiving horn was led through an amplifier to a strip chart recorder to yield the curves shown. Each aperture was centrally cut in a one foot square aluminum plate, and it was assumed that no millimeter-wave radiation escaped the outer boundary of the plate. To minimize extraneous standing wave effects, all of each plate except for the aperture itself was covered with microwave absorber on both sides. The

fixed horn-horn distance in centimeters for each of the four curves in each set is indicated in Fig. 5. On logarithmic ordinate scales, these curves then indicate the relative power detected at the receiving horn as a function of the displacement Z of the aperture along the axis between the horns.

Although highly exaggerated, these curves should suggest the nature of the diffraction effect occurring in the measurement process. The exaggeration arises from the fact that the distance corresponding to Z over which dielectric liquid is actually introduced in a measurement is at most on the order of 1 cm. Consequently, one is concerned only with a central 1 cm segment of the Z-axis for that curve having the appropriate aperture size and horn-horn distance. More precisely, one is concerned with the vertical displacement, at the central point of these curves, between that curve and a similar curve for a horn-horn distance shorter by about 1 cm. For a 10 cm iris, corresponding to the smallest cross-sectional dimension of the sample well of this instrument, the curves suggest that the difference in question is vanishingly small. At least in relation to the beam displacement effect discussed in the following section, this diffraction effect is then presumed to be insignificant. However, it may play a minimal part, as discussed in a later section of the paper, in determining the optimum configuration for operation of the instrument.

Beam Displacement Effects

Transverse motion of the reflected millimeter-wave radiation pattern arising from vertical motion of the reflecting surface has been described as a beam displacement. In a dielectric constant measurement, that surface is the air-dielectric interface. Only that portion of the incident beam actually reflected at that interface is then displaced in the manner indicated. The relative magnitude of that portion is determined by the Fresnel reflection coefficient $\rho\, e^{i\delta}$. Motion of that portion of the beam relative to the cross-section of the receiving horn is expected to yield additional variation in received power.[4]

As with the diffraction effect, measurement of this effect requires separation from effects arising from the dielectric itself. This separation

may be accomplished by replacing the dielectric surface by a floating metal plate and driving the liquid in the manner previously described.

Such "floating plate" measurements are affected by all three of the processes previously described: diffraction, standing wave effects, and beam displacement. However, it was shown in the previous section that diffraction effects as defined herein are negligible. The standing wave pattern may be treated as a periodic oscillation about a mean established by the beam displacement. Such a mean line drawn through the oscillations in experimental "floating plate" curves should then indicate the effect of beam displacement alone.

To represent this effect mathematically, the variation in received power as a function of the height h of the reflecting metal surface may be described by a function $r^2(h)$. At an air-dielectric interface, the relative magnitude of the reflected beam as actually received is then determined by the product $r(d)\rho e^{i\delta}$, replacing h with d. The corresponding power level is then given by $\rho^2 r^2(d)$.

To examine this effect, "floating plate" measurements were made at a frequency of 110 GHz using the pyramidal horns previously described. Relative power levels r^2 as a function of the height h in mm of the reflecting surface for several angles of incidence are shown in Fig. 6, where the indicated curves constitute mean lines drawn through the standing wave patterns. These patterns were essentially constant in amplitude among the curves taken. The ordinate scale for these curves was established using the calibrated millimeter-wave attenuator. Since these curves were found to be very closely symmetrical for ±h, i.e., for the reflecting surface above and below the vertex of the horn axes (h = 0), only the +h portions of the curves are shown.

These curves indicate that the beam displacement effect becomes more pronounced for larger angles of incidence.[4] This result is not surprising, since it is shown in Fig. 4 that the transverse displacement of a ray should be given by $2h \sin \theta_0$. To determine the extent to which this behavior is

34

exhibited by the actual millimeter-wave beam, an attempt was made to fit the experimental curves using the function $r^2(h) = -Kh^2 \sin^2 \theta_0$, as shown on the diagram. On the logarithmic ordinate scale, values for $r^2(h)$ calculated at $h = 2, 3, \ldots, 7$ mm for $K = 3.55$ and 3.85 mm^{-2} are also plotted on Fig. 6. These results indicate that for the small range of transverse displacement considered, the electric field intensity actually received varies with the square of the displacement. The accuracy of the fit shown would not suffice to justify use of that function as a quantitative correction factor. However, the dependence of $r^2(h)$ upon θ_0 as indicated suggests that the interpretation of this effect in terms of the transverse displacement shown in Fig. 4 is probably correct.

More importantly, however, the curves suggest the manner in which beam displacement effects may be minimized. The smallest angle of incidence consistent with other experimental requirements should be employed. Secondly, one should employ a set of transmitting and receiving horns for which transverse displacement yields a minimum variation in received power.

As will be described in a later section, the lensed horns and configuration employed with this instrument were selected on the basis of these criteria. In a subsequent paper of this series, a more complete mathematical description of beam displacement and related effects will be given. That analysis will suggest the difficulties encountered in treating these effects mathematically, thus providing a rationale for the experimental procedures described in the present paper.

Multiple Reflection Effects

In a dielectric constant measurement, one additional effect tends to displace reflected energy transversely with respect to the receiving horn axis. To describe this effect in terms of a ray model, an incident ray may be considered to separate into a first-reflected ray and a transmitted ray at the air-dielectric interface. The transmitted ray, or wave normal, is directed at the real angle of refraction[5] θ'_d towards the metal plate where it is reflected at the same angle back to the interface. A second separation into reflected and transmitted rays then takes place. The emergent ray lies parallel to the first

reflected ray but is displaced transversely by the amount $2d \sin \theta'_d \cos \theta_0$, from the geometry. For subsequent multiply reflected rays, this displacement process is repeated.

This guiding of energy away from the initial point of incidence serves to conserve the tangential components of the energy momentum in the incident beam. A more complete theoretical treatment of this process will be given in a later paper in this series. For the present, it suffices to note that multiple reflections lead to a transverse displacement of the reflected energy similar in character to the beam displacement effect described earlier.

Unlike the beam displacement and other effects described earlier, however, the multiple reflection effect cannot be separated experimentally from the interference effects which yield the reflection coefficient profile. Both types of effect require the presence of a dielectric layer and occur simultaneously. The floating plate measurements illustrated in Fig. 6 do not incorporate multiple reflection effects. No simple experimental estimate of the magnitude of the multiple reflection effect can then be made. Evidence of the magnitude of this effect can only be found in the degree to which the experimental record in a dielectric constant measurement satisfies the theoretical reflection coefficient profile.

To examine the magnitude of that effect qualitatively, the first displacement from double reflection will be less than the beam displacement, i.e., $2d \sin \theta'_d \cos \theta_0 < 2d \sin \theta_0$. Secondly, the energy described by any multiply-reflected ray is attenuated by passage through the dielectric, so that the effect of its displacement will be reduced. In addition, for reflecting surfaces above the vertex of the horn axes the displacements arising from these two mechanisms occur in opposite directions, thus tending to cancel. Finally, multiple-reflection effects are minimized by the same procedures which minimize beam displacement effects, i.e., the use of small angles of incidence and a large surface on the receiving horn.

With regard to multiple reflections, however, it also becomes necessary to insure that those rays which eventually reach the end of the sample well represent negligible energy. It is for this reason, among others, that the sample well in this instrument is elongated in the direction of the plane of incidence. For both displacement effects, the limiting factor with respect to the reception of the total reflected energy is then the area of the receiving horn.

Error Minimization

Of the several sources of instrumental error described, the beam displacement effect appears to be both the most prominent and the most amenable to control. Standing wave and diffraction effects are minimized, for the most part, in the basic construction of the instrument. Multiple reflection effects, on the other hand, are minimized by the same procedures which minimize beam displacement effects.

These procedures consist of insuring that as much as possible of the energy reflected from the air-dielectric-metal configuration is actually received. To accomplish that end for a given set of horns, a minimum angle of incidence should be employed. The optimum set of horns will consist of a transmitting horn yielding a minimum beam width and divergence, and a receiving horn of large cross-section and a flat response. In basing the instrument design on direct experimental evidence, however, the optimum horn system was first selected, and then the behavior of that system with respect to both the angle of incidence and the horn-horn distance was examined.

To select the optimum horn system, five combinations of three types of horn were studied. These horns consisted of (A) a commercial pyramidal horn designed for the 90-140 GHz band, (B) horn A with an attached plano-convex lens, and (C) a commercial conical lensed horn of 3-inch aperture designed for the same band. The horns of type A were those employed in obtaining the data illustrated in Figs. 5 and 6. The lens attached to obtain horn type B was of 3 cm diameter, constructed from a commercial polymeric material

and designed from a standard lens formula.[6] The lens was attached on its flat side by a shallow notch fitting the end of the horn.

The five combinations of transmitting-receiving horns examined were as follows: (a) A-A, (b) B-A, (c) B-B, (d) B-C, and (e) C-C. To examine these horns, the transmitting and receiving systems were mounted in-line on an optical bench to provide direct transmission. For each combination, measurements were then made of the variation in received power P with transverse displacement ℓ of the receiving horn relative to the transmitting horn axis. For four of these combinations, results of these measurements at an operating frequency of 140 GHz are illustrated in Fig. 7.

The curves a, b, and c represent the effect of no lenses, a small lens on the transmitting horn, and small lenses on both horns, respectively. Narrowing of the radiation patterns of both horns in this manner appears to yield a simple narrowing of the response curve of the horn-horn system with respect to transverse displacement. (The abscissa scale of Fig. 7 was located only approximately, and appears to be offset from the transmitting horn axis.)

Curve d represents the effect of using a small lens on the transmitting horn and a lensed horn of relatively large aperture on the receiver. From the interpretation given earlier, this system should yield a more constant response with respect to transverse displacement. Curve d indeed contains a relatively flat segment. Additional effects appear at large displacements, however, as shown by the dip in curve d. The horn system C-C containing two conical lensed horns yields a curve (not illustrated) with a very deep central dip, rendering that system impracticable.

The horn combination B-C, whose response to transverse displacement is shown in curve d of Fig. 7, was then chosen for use in this instrument. As can be seen in that curve, there occurs an optimum range of transverse displacement over which the received power remains relatively constant. When this horn combination is employed in the interferometer, there will then exist an optimum height for the dielectric-metal interface. Starting from that initial height, power variations arising from the beam displacement effect are minimized.

To determine the optimum configuration of the instrument with respect to the angle of incidence and horn-horn distance H, a series of floating plate measurements was made at 140 GHz using the horn combination B-C. As noted previously, such measurements are affected by diffraction effects, standing waves, and beam displacement. As such, these measurements indicate the degree to which such effects may constitute sources of error in dielectric constant measurements.

For the values H = 30 cm and 40 cm and θ_0 = 30°, 40°, and 50°, results of these floating plate measurements are shown in Fig. 8, where the ordinate scale is simply that of the recorder paper and has no absolute significance. Except for the use of a different set of horns (and a higher operating frequency), these curves were obtained by the same procedures used to obtain the curves of Fig. 6.

In Fig. 8, however, the curves are reproduced just as taken, including the standing wave patterns. Mean lines drawn through these patterns as was done in obtaining Fig. 6 would in this case yield essentially flat, straight lines. To that extent, beam displacement and diffraction effects have then been eliminated as sources of error in this instrument.

The oscillations in Fig. 8 are identified as standing wave patterns on the basis of their wavelengths. The lack of complete symmetry in some of the curves suggests that other effects may also be occurring. The curves also suggest that the amplitude of the standing wave patterns may be affected by the angle of incidence and the horn-horn distance. A part of the differences in amplitude may have resulted from changes in tuning of the millimeter-wave components. In any case, the curves indicate that for the configuration θ_0 = 30° and H = 30 cm, the standing wave pattern is least in amplitude, and symmetrical. That configuration was then adopted for use in this instrument.

5. SUMMARY

An apparatus designed for free-space, interferometric measurements in the millimeter-wave region of the complex dielectric constant of liquids has been described. Fundamental sources of error including vibration and klystron noise have been minimized in the basic design of the instrument and its associated electronics. A formal system for relating power and dielectric thickness data in the experimental record to a theoretical reflection coefficient has been given.

Additional sources of error arising from the quasi-optical nature of the millimeter-wave radiation have been identified. In addition to standing wave effects, there occur diffraction, beam displacement, and multiple reflection effects. Experimental data which exhibit techniques for minimizing these sources of error have been presented. The floating plate measurement constitutes a means of testing the operation of the instrument and the magnitude of such errors with an ease equal to that of a dielectric constant measurement.

Of the sources of error described, however, the influence of multiple reflection and standing wave effects can only be determined from the degree to which experimental data may be adequately described theoretically. To the extent to which it is significant, the multiple reflection effect may tend to cancel the beam displacement effect, if an appropriate initial height of the dielectric-metal interface is chosen. The phase variations over successive multiply-reflected rays may also tend to cancel   standing wave effects. That a measurable standing wave effect using a floating plate apparently becomes insignificant in a dielectric constant measurement, in which multiple reflections occur, has been noted.

In subsequent publications, theoretical expressions describing the reflection coefficient profile will be derived, the mathematical techniques necessary to obtain the complex dielectric constant from such expressions will be described, and a series of experimental data from which an error analysis may be carried out will be presented.

ACKNOWLEDGMENTS

REFERENCES

1. W. S. Lovell, Paper I.

2. W. E. Vaughan, W. S. Lovell, and C. P. Smyth, J. Chem. Phys. $\underline{36}$, 535 (1962).

3. W. E. Vaughan, K. Bergmann, and C. P. Smyth, J. Phys. Chem. $\underline{65}$, 94 (1961).

4. M. Schünzel and M. Stockhausen, Zeit. Angew. Phys. $\underline{21}$, 508 (1966).

5. M. Born and E. Wolf, Principles of Optics (Pergamon, 1959), pp. 612-3.

6. A. F. Harvey, Microwave Engineering (Academic Press, 1963), p. 648.
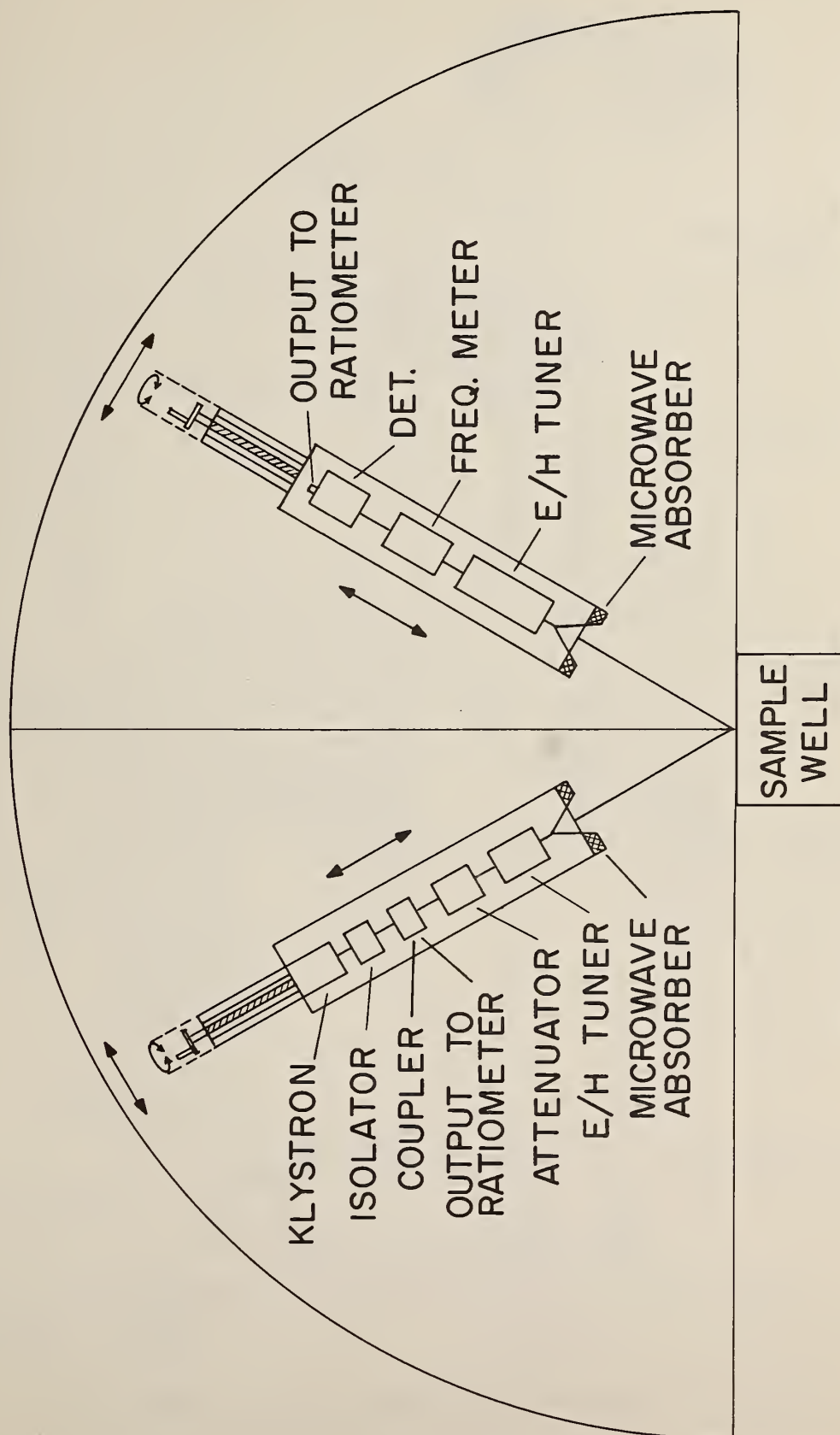
Figure 1: Millimeter-wave interferometer: Positioning and motional adjustments of millimeter-wave components.
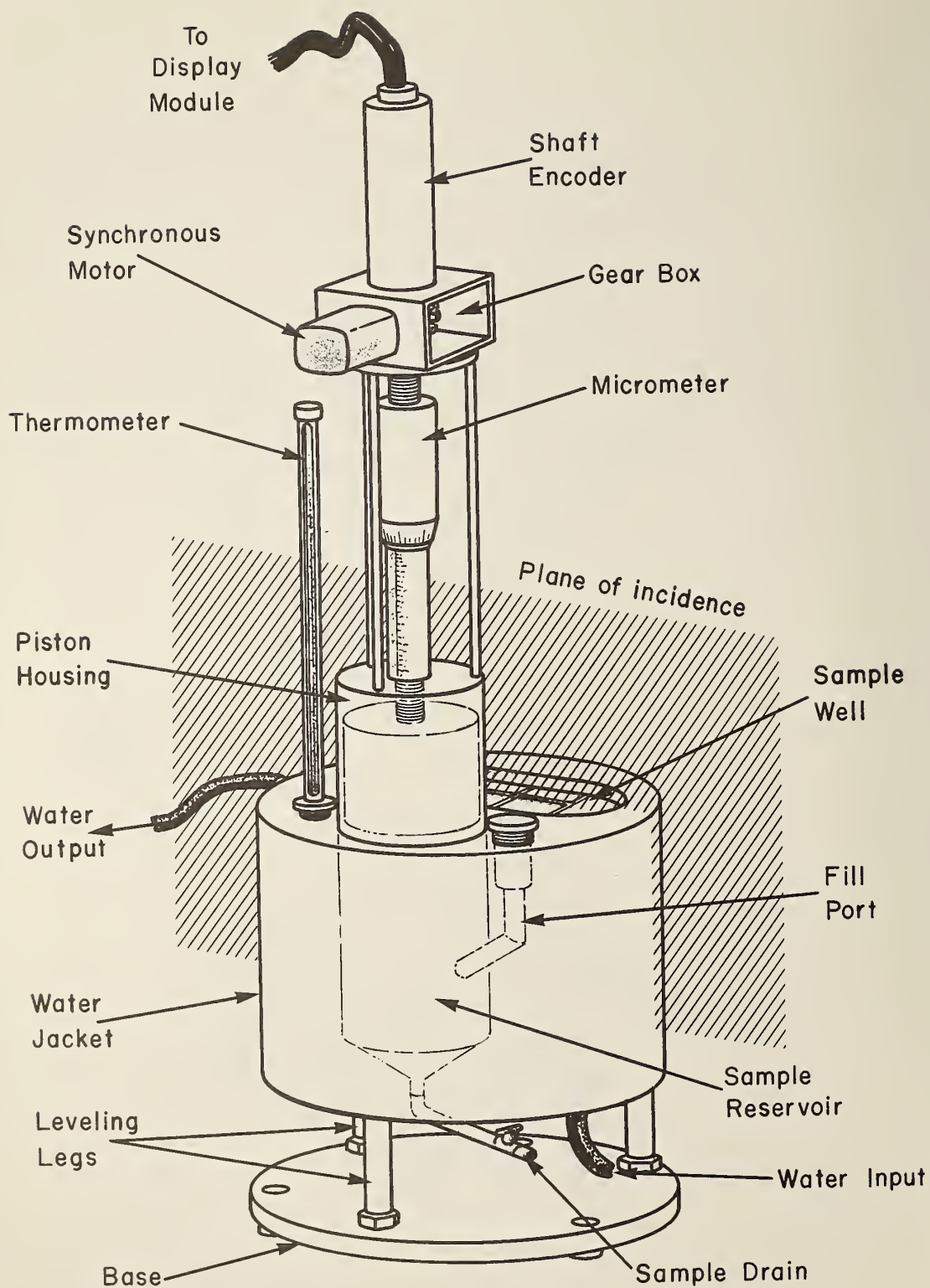
Figure 2:   Millimeter-wave interferometer: sample cell.
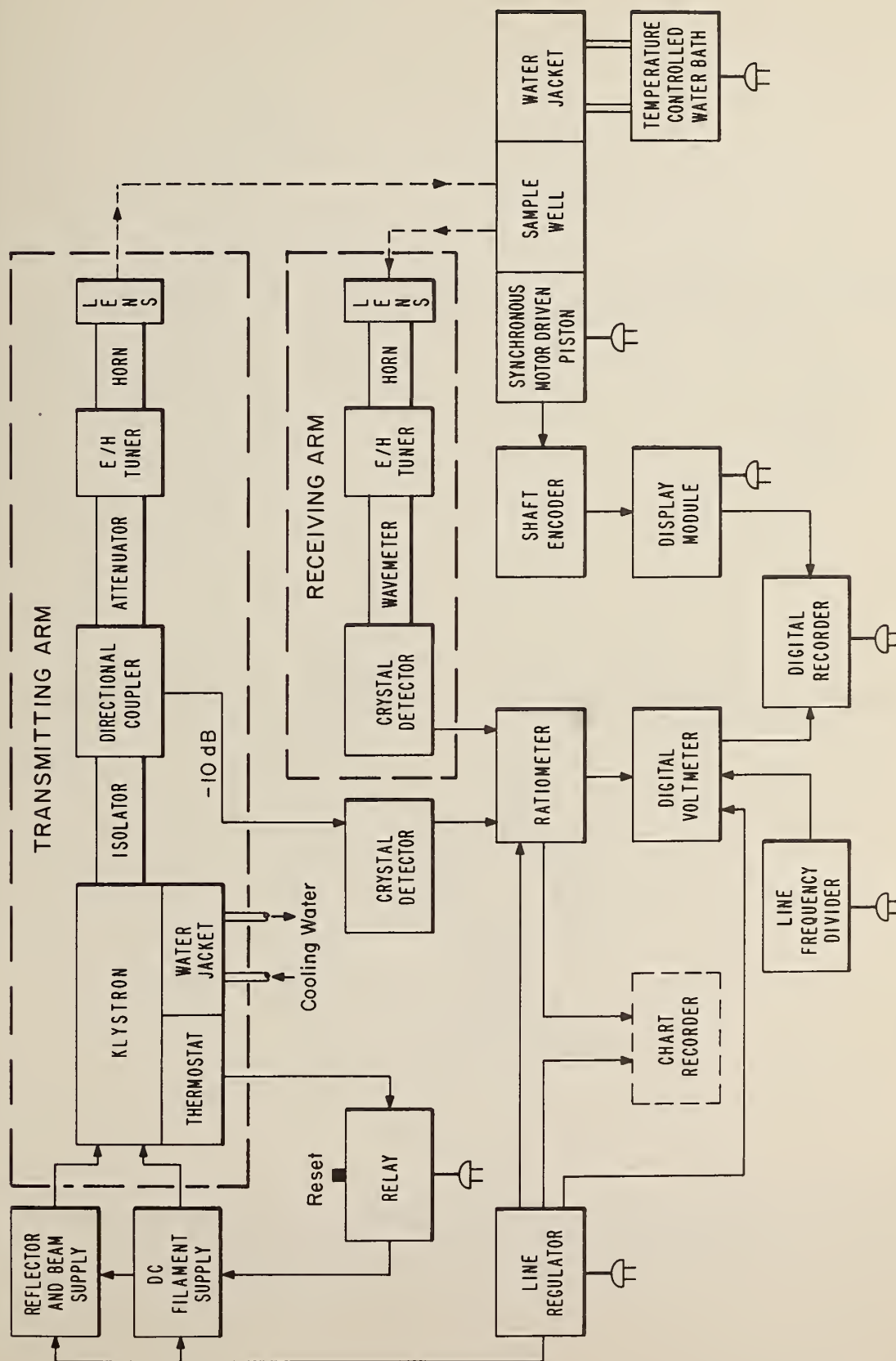
Figure 3: Millimeter-wave interferometer: block diagram of millimeter-wave components, sample well, and associated electronic equipment.
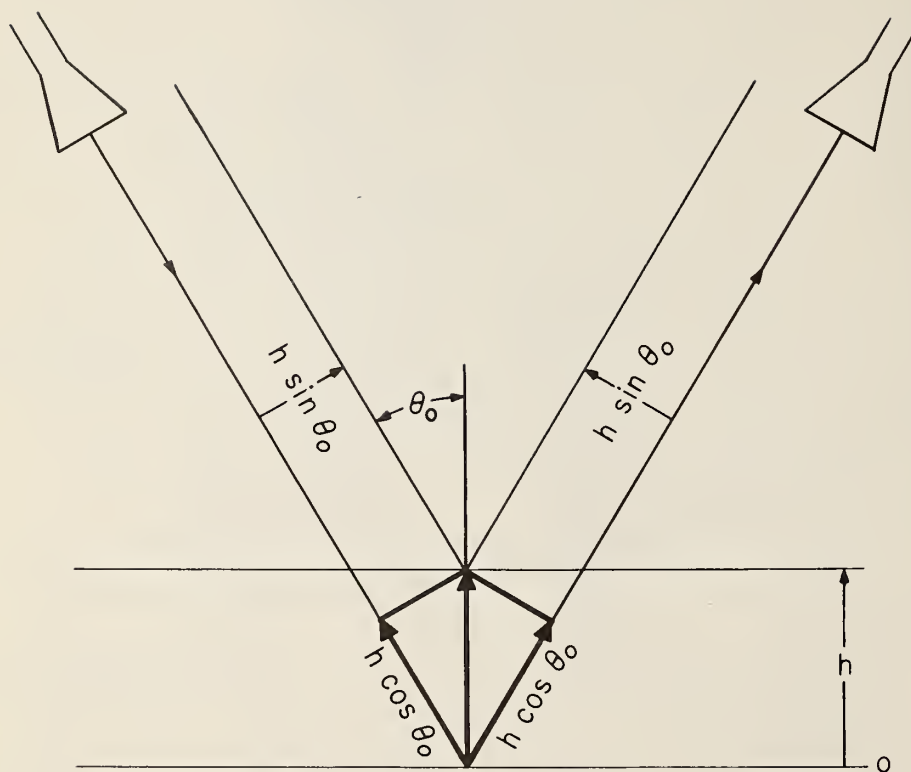
Figure 4: Geometrical model of measurement process showing longitudinal and transverse motion of reflected ray.
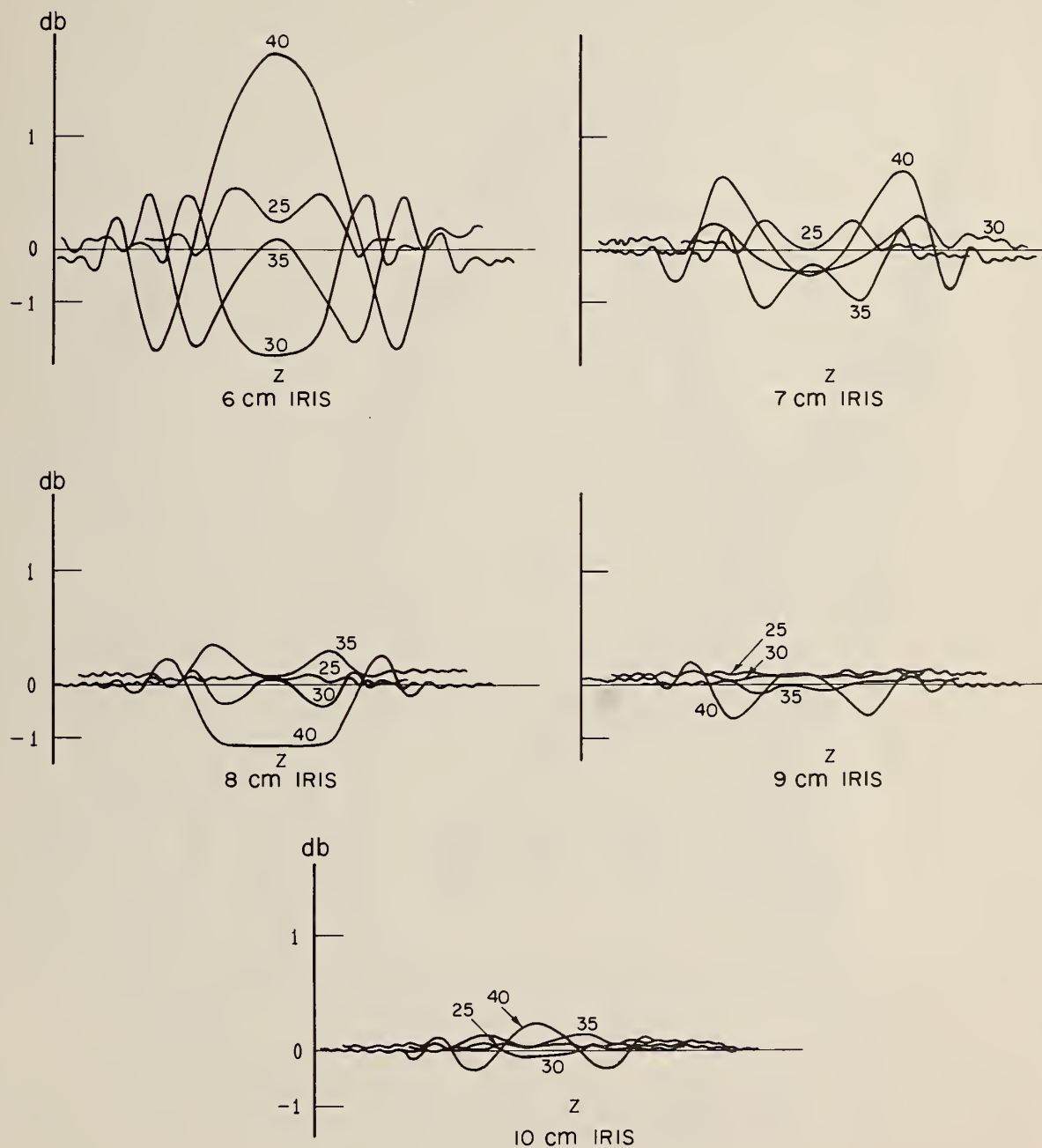
Figure 5: Diffraction effects at 110 GHz for irises of 6-10 cm diameter. Curves show the variation in received power as the iris is translated on the axis Z between the horns for the total horn-horn distance in cm indicated on each curve.

47
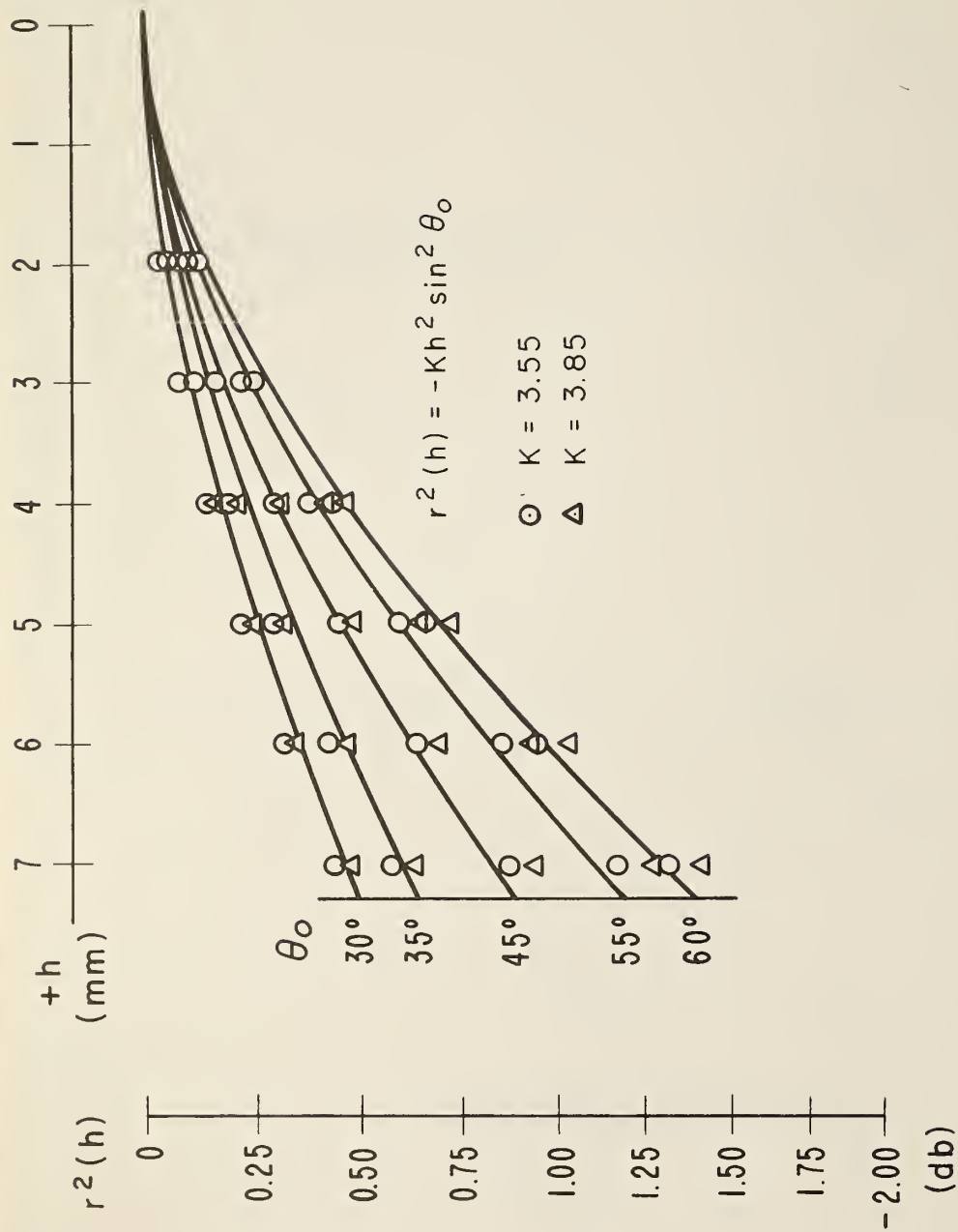
Figure 6: Relative power $r^2(h)$ measured as a reflecting surface is raised the distance h above the vertex of the horn axes shown in Fig. 4. The curves represent mean lines drawn through the accompanying standing wave patterns. The points are calculated from the equation shown for $K = 3.55$ and 3.85 mm^{-2}.
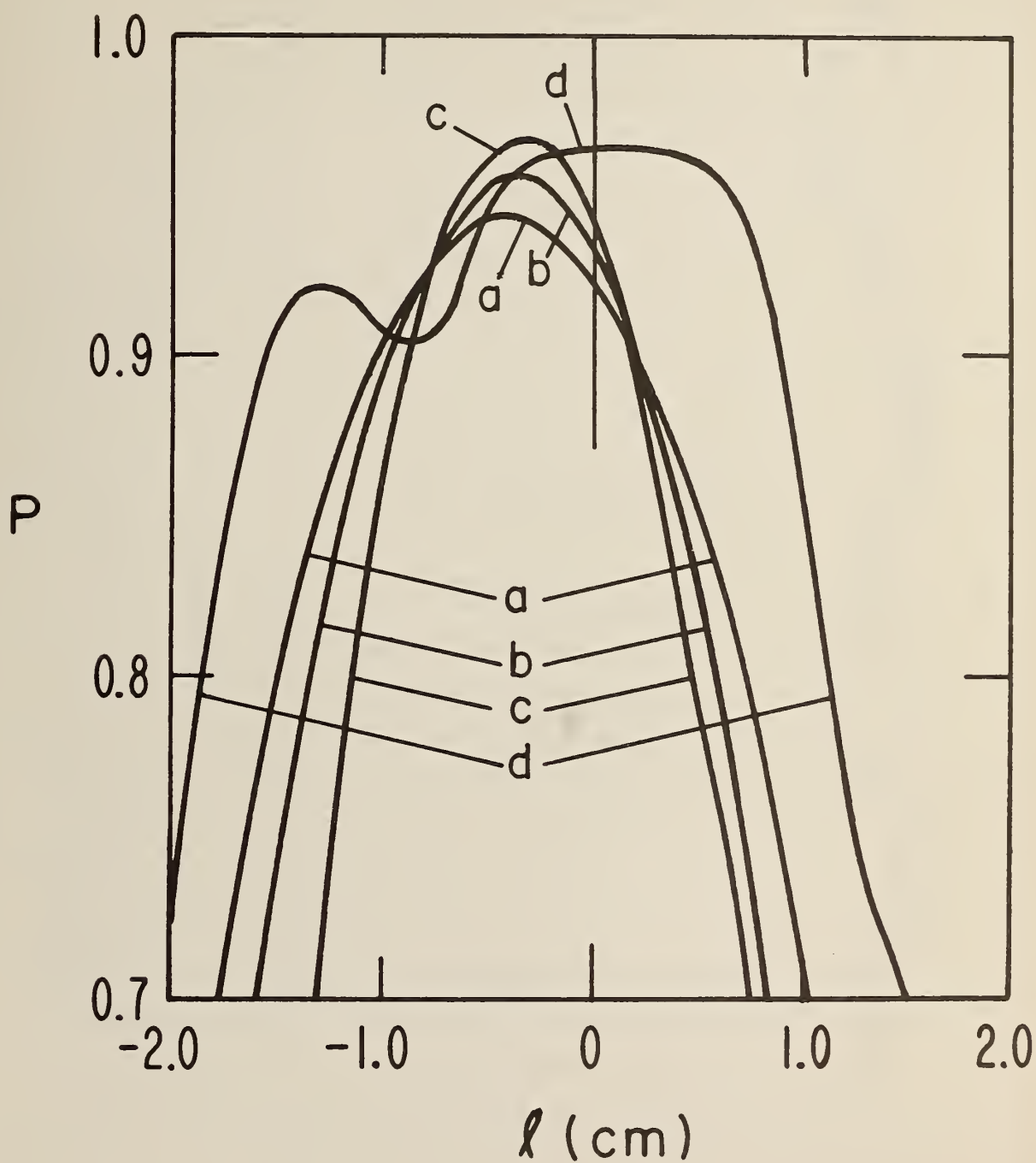
Figure 7: Relative power P as a function of transverse displacement ℓ for four combinations of transmitting and receiving horns as described in the text.

49
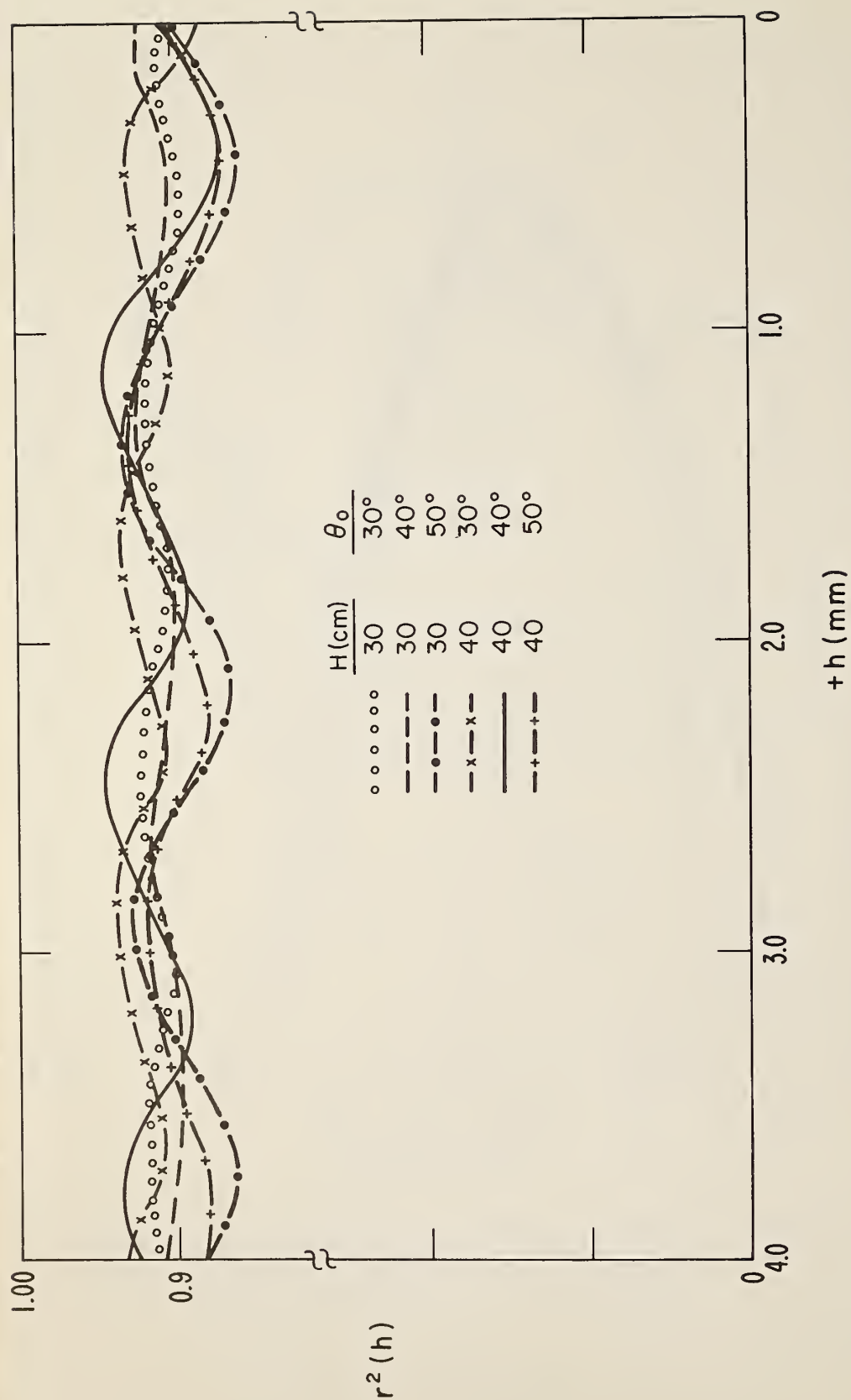
Figure 8: Floating plate measurements using the horn combination B-C as described in the text, corresponding to curve d of Fig. 7. The curves were taken at six different combinations of horn-horn distance H and angle of incidence θ_0 as shown in the table.

H(cm)	θ_0
30	30°
30	40°
30	50°
40	30°
40	40°
40	50°

Interferometric Measurements of the Complex

Dielectric Constant of Liquids

III. Derivation of the Absolute Reflection Coefficient

William S. Lovell

and

Lynn M. Thiel

ABSTRACT

For measurements of the complex dielectric constant
of liquids by free-space reflection and interference of electro-
magnetic radiation, a theoretical reflection coefficient for the
air-dielectric-metal configuration is derived. The derivation
is based on a model which treats multiple reflections within
the dielectric explicitly. As an extension of earlier theory,
this reflection coefficient incorporates effects of (1) imperfect
reflections at the dielectric-metal interface, together with
other losses, and (2) radiation sources presenting nonplanar
wavefronts and having finite bandwidths. Effects arising from
a finite sample or receiving surface are also discussed.

1. INTRODUCTION

A previous paper[1] (I) has shown that in applications of the free-space, interferometric measurement technique, the complex dielectric constant of liquids cannot be determined accurately using the "perfect square approximation" of the equation

$$R(d) = \frac{\rho^2 - 2\rho \cos(2\beta d + \delta)e^{-2\alpha d} + e^{-4\alpha d}}{1 - 2\rho \cos(2\beta d - \delta)e^{-2\alpha d} + \rho^2 e^{-4\alpha d}} , \qquad (1)$$

where the reflected power R is given as a function of the dielectric sheet thickness d. This perfect square approximation treats the phase shift δ of electromagnetic radiation upon reflection at the air-dielectric interface as equal to π. It was shown that the errors introduced by this procedure are unacceptable except in estimating ϵ^*.

The ability of Eq. (1) to describe the reflection process adequately has not been shown experimentally. An experimental test of Eq. (1) requires both an apparatus sufficiently free of effects not described by a reflection coefficient and an explicit treatment of Eq. (1) not involving mathematical approximation. Such an apparatus, from which experimental data should conform to an adequate theoretical treatment, has been described in the second paper (II) of this series.[2]

In the present paper, certain modifications of Eq. (1) will be proposed. The resulting expression incorporates Eq. (1) as a limiting case; hence, explicit calculation using the proposed expression provides a test of the degree of validity of Eq. (1). The actual manner of carrying out such calculations will be described in the following paper in this series.

Recent derivations[3-5] of Eq. (1) have been based on the use of boundary conditions at the air-dielectric interface which incorporate implicitly the effects of multiple reflections within the dielectric. These reflections are treated explicitly in the present paper in order to present more detailed description of the reflection process. In addition, these recent derivations have employed, either explicitly or implicitly, the assumptions that (1) there is no loss of power in the experimental apparatus and (2) the incident radiation has a single

52

wavelength and is propagated at a single angle of incidence. In the present paper, an alternative set of assumptions is employed: (1) the loss of power in the system is appreciable and includes the effect of imperfect reflections at the dielectric-metal interface,[2] and (2) the incident radiation has a continuous distribution of wavelengths and is propagated at a continuous distribution of angles of incidence. Together with the explicit multiple-reflection treatment, these modifications have been found necessary in order to describe conditions existing in the experimental apparatus.

2. DERIVATION FOR THE IDEAL CASE

The air, dielectric, and metal media in Fig. 1 are designated by the numbers 1, 2, and 3, respectively. At the coplanar interfaces between these media, each reflection coefficient r_{ij} and transmission coefficient t_{ij} is denoted by selecting the proper subscripts corresponding to the media defining the interface. The complex angle of refraction is represented by θ_d and the ith complex propagation vector by k_i. Notice that $-k_0 = k_1 = k_4 = k_7 = \dots$, $k_d = k_2 = k_5 = k_8 = \dots$, and $-k_d = k_3 = k_6 = k_9 = \dots$. Normal propagation within the dielectric is then described by the complex propagation constant $k_d \cos \theta_d$.

Amplitudes of the successive electric vectors in the air and dielectric media are described by repeated application of the reflection and transmission coefficients[5] and represented by the equations

$$E_1 = r_{12} E_0$$

$$E_{3n-1} = t_{12} E_0 \left[r_{23} r_{21} \exp(-2k_d \cos \theta_d d) \right]^{n-1}$$

$$E_{3n} = t_{12} r_{23} E_0 \exp(-2k_d \cos \theta_d d) \left[r_{23} r_{21} \exp(-2k_d \cos \theta_d d) \right]^{n-1}$$

$$E_{3n+1} = t_{12} r_{23} t_{21} E_0 \exp(-2k_d \cos \theta_d d) \left[r_{21} r_{23} \exp(-2k_d \cos \theta_d d) \right]^{n-1},$$

$$n = 1, 2, \dots ,$$

(2)

where d is the dielectric thickness. The complex reflection coefficient is defined[6] as

$$\frac{E_R}{E_0} = \sum_{n=0}^{\infty} \frac{E_{3n+1}}{E_0} .$$

(3)

53

Since $\left| r_{23} r_{21} \exp(-2k_d \cos\theta_d d)\right| < 1$, the infinite series in Eq. (3) converges absolutely and uniformly[7] to a sum which after rearrangement becomes

$$\frac{E_R}{E_0} = \frac{r_{12} + r_{23}(t_{12}t_{21} - r_{21}r_{12})\exp(-2k_d \cos\theta_d d)}{1 - r_{21}r_{23}\exp(-2k_d \cos\theta_d d)} . \tag{4}$$

Applying the principle of reversibility (which implies $r_{12} = -r_{21}$ and $t_{12}t_{21} - r_{21}r_{12} \equiv 1$) and the definition

$$k_d \cos\theta_d \equiv \alpha + i\beta , \tag{5}$$

then Eq. (4) takes the form

$$\frac{E_R}{E_0} = \frac{r_{12} + r_{23}\exp[-2d(\alpha + i\beta)]}{1 + r_{12}r_{23}\exp[-2d(\alpha + i\beta)]} . \tag{6}$$

Let the reflection at the air-dielectric interface be described by the Fresnel reflection coefficient so that $r_{12} = \rho e^{i\delta}$. If it is assumed that there is no loss of power in the system, which implies in part that the reflection at the dielectric-metal interface is perfect, then $r_{23} = -1$ and Eq. (1) is obtained by defining $R(d) = \left|E_R/E_0\right|^2$. If losses in the system are assumed, let $r_{23} = \sigma e^{i\psi}$, where $\sigma e^{i\psi}$ is a complex reflection coefficient with the amplitude $\sigma < 1$, then in this case

$$R(d) = \frac{\rho^2 + 2\sigma\rho\cos(2\beta d + \delta - \psi)e^{-2\alpha d} + \sigma^2 e^{-4\alpha d}}{1 + 2\sigma\rho\cos(2\beta d - \delta - \psi)e^{-2\alpha d} + \sigma^2\rho^2 e^{-4\alpha d}} , \tag{7}$$

and $R(d)$ is defined to be the theoretical reflection coefficient. It should be noted that Eq. (7) reduces to Eq. (1) in the case that $\sigma \equiv 1$ and $\psi \equiv \pi$. Parenthetically, it may be noted that if $r_{23} = -r_{21} = -\rho e^{i\delta}$, i.e., medium 3 in Fig. 1 is replaced by air, then Eq. (6) reduces to the Airy formula.[8]

3.   THE FINITE SAMPLE AND/OR RECEIVING SURFACE

In evaluating the infinite series in Eq. (3), it is implied that the reflected energy as measured will incorporate equally all of the electric vectors E_{3n+1}. In principle, this situation could only be realized on condition that (1) the dielectric sample and reflector are infinite in length, (2) the dimensions of the receiving surface parallel to the plane of constant phase are infinite, and (3) the receiving surface has a uniform response over its cross-section. In practice, it is then necessary either to approximate these conditions experimentally or to give an alternative treatment of the reflection coefficient.

In (II), the detailed mechanisms by which reflected energy may not be received were discussed, and it was shown that a reasonable approximation to these conditions may be achieved. The steps required to achieve that approximation include (1) use of a sample well of sufficient area so that the receiving horn constitutes the limiting factor with respect to reception of reflected energy and (2) design of the transmitting horn, receiving horn, and interferometer configuration such that the diffraction, standing wave, beam displacement, and multiple reflection effects discussed in (II) are minimized.

For now, it is the intent to present a method by which failure to receive all of the reflected energy may be described mathematically. As such, this treatment is concerned only with the multiple reflection and beam displacement effects.

With respect to multiple reflections, the transverse displacement between the reflected rays k_1, k_4, k_7, etc., shown in Fig. 1 is given by $2d \sin \theta_d' \cos \theta_0$. Such reflections within the dielectric yield a propagation of energy tangentially to the dielectric surface. That such propagation must occur by some means is apparent from the fact that the incident electromagnetic energy propagates with momentum components tangential to the dielectric surface. In typical derivations of the reflection coefficient using Maxwell boundary conditions[9], this energy transfer is not obvious since only the normal component of the Poynting vector is treated.

With reference to Fig. 1, consider a receiving horn oriented at the angle of reflection such that the ray k_1 falls within one edge of its cross-section, but some later ray, say $k_{n'}$, just misses the opposite edge. Assuming that the horn response is uniform over its cross-section, a reflection coefficient which describes the resultant effect (in the ray approximation) may be derived by truncating the series in Eq. (3) at the $(n'-1)\underline{\text{th}}$ term. The ratio of that sum[10] to the sum of the infinite series will be identical to the ratio of the corresponding reflection coefficient, which implies

$$R'(d)/R(d) = \left| 1 - [r_{23}r_{21}\exp(-2k_d\cos\theta_d d)]^{n'} \right|^2 \geq \left[1 - |r_{23}r_{21}\exp(-2k_d\cos\theta_d d)|^{n'} \right]^2.$$

(8)

It then follows that

$$1 \geq R'(d)/R(d) \geq \left[1 - (\sigma\rho e^{-2\alpha d})^{n'} \right]^2$$

(9)

substituting for r_{23} and r_{21} as before.

For small σ and ρ and for large α, i.e., for weak reflections at the dielectric-metal interface and high loss dielectrics, the effect of multiple reflections will be minimized. The consequences of not receiving the rays for which $n > n'$ will be reduced since they will represent negligible energy. Consistent with the discussion given in (II), multiple reflection effects are minimized at smaller angles of incidence, since n' is thereby increased. Without prior knowledge of the complex dielectric constant, however, n' could not be caluclated, and in any case the calculation would be impracticable, as is shown below. For that reason, the experimental procedures described in (II) are employed to take account of multiple reflections.

To describe a response distribution at the receiving horn, let $r_n(d) = r(d-nx)$ be some distribution function for which x is defined in Fig. 2. The quantity $(d-x)$ represents the change in height of the reflecting surface required to place a ray such as k_4 at an equivalent position by simple reflection instead of refraction and reflection. For the ray k_{3n+1}, that same height

is given by (d -nx), where n is the ray index used previously, but now $0 \leq n$. From Fig. 2, it can be seen that

$$x(d) = d \; \frac{\tan \theta'_d}{\tan \theta_0} \; , \tag{10}$$

where θ'_d is the real angle that the wave normal makes with the surface normal.[11]

To account for the finite horn dimensions with greater generality, consider a characteristic function $\chi_{(n_1, n_2)}$ defined by

$$\chi_{(n_1, n_2)} (n) \equiv \begin{cases} 1, \text{ if } n_1 \leq n \leq n_2, \\ 0, \text{ otherwise} \end{cases} \tag{11}$$

where n_1 and n_2 are the indices of the first and last rays received, respectively. These indices are dependent not only on the dielectric thickness but also on the horn-to-horn distance, dimensions of the horn, λ_0, and θ_0. Such dependence arises from the beam displacement as well as the multiple reflection effects. The infinite series of Eq. (3) now takes the form

$$\frac{E_R}{E_0} = \frac{\sum\limits_{n=0}^{\infty} \frac{E_{3n+1}}{E_0} \chi_{(n_1, n_2)} r_n}{\sum\limits_{n=0}^{\infty} \chi_{(n_1, n_2)} r_n} = \frac{\sum\limits_{n=n_1}^{n_2} \frac{E_{3n+1}}{E_0} r_n}{\sum\limits_{n=n_1}^{n_2} r_n} \; . \tag{12}$$

Success in finding a closed form for the series of Eq. (12) depends on the form of the terms. Experimental examples of r have been given in (II).

The experimental minimization of beam displacement and multiple reflection effects requires construction[12] of a receiving horn which is large enough to approximate a horn of infinite dimensions with a flat response. With reference to the experimental apparatus previously described,[2] this is the approach taken in this paper and is valid for the range of dielectrics under consideration.

4. DERIVATION TO INCLUDE A DISTRIBUTION IN λ_0 AND θ_0

Instead of assuming that the incident radiation has the single wave-length λ_0 and is propagated at the single angle of incidence θ_0, assume that the normal point (θ_0, λ_0) gives the maximum of a continuous frequency function defined over the set

$$S = \{(\theta, \lambda) \mid \theta_0 - \frac{\pi}{2} \leq \theta \leq \theta_0 + \frac{\pi}{2}, \ 0 \leq \lambda < \infty \}. \tag{13}$$

Let x and y be continuously differentiable functions of θ and λ, respectively, and let (x, y) map S onto the extended real plane R*. Assume (x, y) is normally distributed and, for the sake of generality, also dependently distributed. The normal frequency function [13, 14] of (x, y) is then given by

$$W(x, y) = \frac{\exp\left\{\frac{-1}{2(1-\tau^2)}\left[\left(\frac{x-\mu_x}{\sigma_x}\right)^2 - 2\tau\left(\frac{x-\mu_x}{\sigma_x}\right)\left(\frac{y-\mu_y}{\sigma_y}\right) + \left(\frac{y-\mu_y}{\sigma_y}\right)^2\right]\right\}}{2\pi\sigma_x\sigma_y\sqrt{1-\tau^2}}, \tag{14}$$

where the parameters μ_x, σ_x, μ_y, σ_y, and τ are the mean and standard deviation of x, the mean and standard deviation of y, and the correlation coefficient between x and y. The variable (θ, λ) cannot be normally distributed since S is not equal to R* as is the range of (x, y). There exist one-to-one functions x and y on $[\theta_0 - \frac{\pi}{2}, \ \theta_0 + \frac{\pi}{2}]$ and $[0, \infty)$ respectively onto R* which satisfy:

$$x(\theta_0 - \frac{\pi}{2}) = -\infty, \quad x(\theta_0 + \frac{\pi}{2}) = \infty,$$

and $\hspace{10cm}$ (15)

$$y(0) = -\infty, \quad y(\infty) = \infty.$$

For simplicity, let

$$\mu_x = x(\theta_0) = 0 \qquad \text{and} \qquad \mu_y = y(\lambda_0) = 0 \tag{16}$$

and for practicability let

$$x'(\theta_0) = 1 \quad \text{and} \quad y'(\lambda_0) = 1. \tag{17}$$

Also, since the radiating horn contains a plane of symmetry perpendicular to the plane of incidence, let

$$x(\theta_0 - \Delta\theta) = -x(\theta_0 + \Delta\theta) \tag{18}$$

for all $-\dfrac{\pi}{2} \le \Delta\theta \le \dfrac{\pi}{2}$ where $\Delta\theta \equiv \theta_0 - \theta$. Since the distribution of λ may be regarded as symmetric with respect to λ_0 for narrow bandwidths, also let

$$y(\lambda_0 - \Delta\lambda) \approx -y(\lambda_0 + \Delta\lambda) . \tag{19}$$

for small $\Delta\lambda$ where $\Delta\lambda \equiv \lambda_0 - \lambda$.

Let $w(\theta, \lambda)$ be the density function for (θ, λ). Since the Jacobian[15, 16] of x, y with regard to θ and λ is $J = x'(\theta) y'(\lambda)$, then

$$w(\theta, \lambda) = W[x(\theta), y(\lambda)] x'(\theta) y'(\lambda) . \tag{20}$$

The theoretical reflection coefficient with the assumed distribution (14) is obtained by applying the well known weighted mean formula.[17] For this purpose let $f = f(\theta, \lambda;d)$ be defined by the function on the right-hand side of Eq. (7). Then since f is continuous and bounded and w is a frequency function,

$$R(d) = \frac{\displaystyle\iint_S f(\theta, \lambda;d)\, w(\theta, \lambda)\, d\theta\, d\lambda}{\displaystyle\iint_S w(\theta, \lambda)\, d\theta\, d\lambda} = \int_0^\infty \int_{\theta_0 - \frac{\pi}{2}}^{\theta_0 + \frac{\pi}{2}} f(\theta, \lambda;d) w(\theta, \lambda)\, d\theta\, d\lambda \tag{21}$$

exists where $\displaystyle\iint_S w(\theta, \lambda)\, d\theta\, d\lambda = 1$; $R(d)$ is defined to be the absolute reflection coefficient.

59

Practical application of Eq. (21) requires explicit functions for x and y. Possibly there exists a number of functions which satisfy conditions (15) through (19) and have continuous first derivatives. However, for reasonable functions, the distribution is expected to be insensitive to such functions for proper choices of σ_x and σ_y. Two functions which might be considered are $\tan(\theta - \theta_0)$ and $\lambda_0 \ln(\lambda \lambda_0^{-1})$.

5. SUMMARY

For interferometric, millimeter-wave measurements of the complex dielectric constant of liquids in an air-dielectric-metal configuration, a theoretical reflection coefficient adequate to describe quantitatively the experimental reflection coefficient profile is required. In deriving that reflection coefficient, the occurrence of imperfect reflections at the dielectric-metal interface, as well as other energy loss mechanisms, must be considered.

Explicit treatment of the multiple reflections occurring in the reflection-interference process by which the dielectric constant is measured discloses a need for either (1) a specially designed system of transmitting and receiving horns to insure reception of all reflected energy or (2) a mathematical description of the beam displacement and multiple reflection processes by which energy would otherwise be lost. The first of these alternatives was determined to be the more practicable. However, a formalism is presented by which such effects may be incorporated into the theoretical reflection coefficient.

A more realistic radiation source yielding a nonplanar wavefront and having a finite bandwidth is considered in Eq. (21). For this, a normal distribution in (x, y) was assumed above. It was chosen because the distribution of $\tan(\theta - \theta_0)$ and $\lambda_0 \ln(\lambda \lambda_0^{-1})$ have been observed to be approximately normal and the normal frequency function has been extensively studied. It must be noted, however, that with the appropriate parameters, use of almost any distribution which is symmetric and monotonically increasing as (θ_0, λ_0) is approached is better than the assumption that the radiation has a single

wavelength λ_0 and is propagated at the single angle of incidence θ_0. It might very well be that there exist other distributions which are closer to reality than the one considered above. The solution of the reflection coefficient expression given in Eq. (21) will be discussed in a later paper.

REFERENCES

1. W. S. Lovell, Paper I.

2. W. S. Lovell, Paper II.

3. W. E. Vaughan, K. Bergmann, and C. P. Smyth, J. Phys. Chem. 65, 94 (1961).

4. W. E. Vaughan, Thesis, Princeton University (1960).

5. M. Yasumi, Bull. Chem. Soc. Japan 24, 53 (1951).

6. W. Pfister and O. H. Roth, Hochfrequenztechn. U. Elektroak. 51, 156 (1938).

7. E. Hille, Analytic Function Theory (Blaisdell Publishing Co., Inc., 1965) Vol. I, pp. 102, 107.

8. M. Born and E. Wolf, Principles of Optics (Pergamon Press, 1959), pp. 60-61, 322-325.

9. J. A. Stratton, Electromagnetic Theory (McGraw-Hill, 1941), p. 496

10. L. B. W. Jolley, Summation of Series (Dover, 1961), 2nd Rev. Ed., pp. 2-3.

11.. Reference 9, p. 502.

12. That the loss of reflected energy can be significant, but can also be eliminated by appropriate horn design, is apparent from a comparison of Figs. 6 and 8 of Ref. 2.

13. G. U. Yule and M. G. Kendall, An Introduction to the Theory of Statistics (Hafner Publishing Co., 1950), pp. 238-239.

14. P. G. Hoel, Introduction to Mathematical Statistics (John Wiley & Sons, Inc., 1947), p. 150.

15. J. Edwards, A Treatise on the Integral Calculus (Chelsea Publishing Co., 1954), Vol. 1, pp. 825-826.

16. W. H. Fleming, Functions of Several Variables (Addison-Wesley Publishing Co., Inc., 1965), p. 175.

17. M. Fisz, Probability Theory and Mathematical Statistics (John Wiley & Sons, 1963), pp. 64-80.
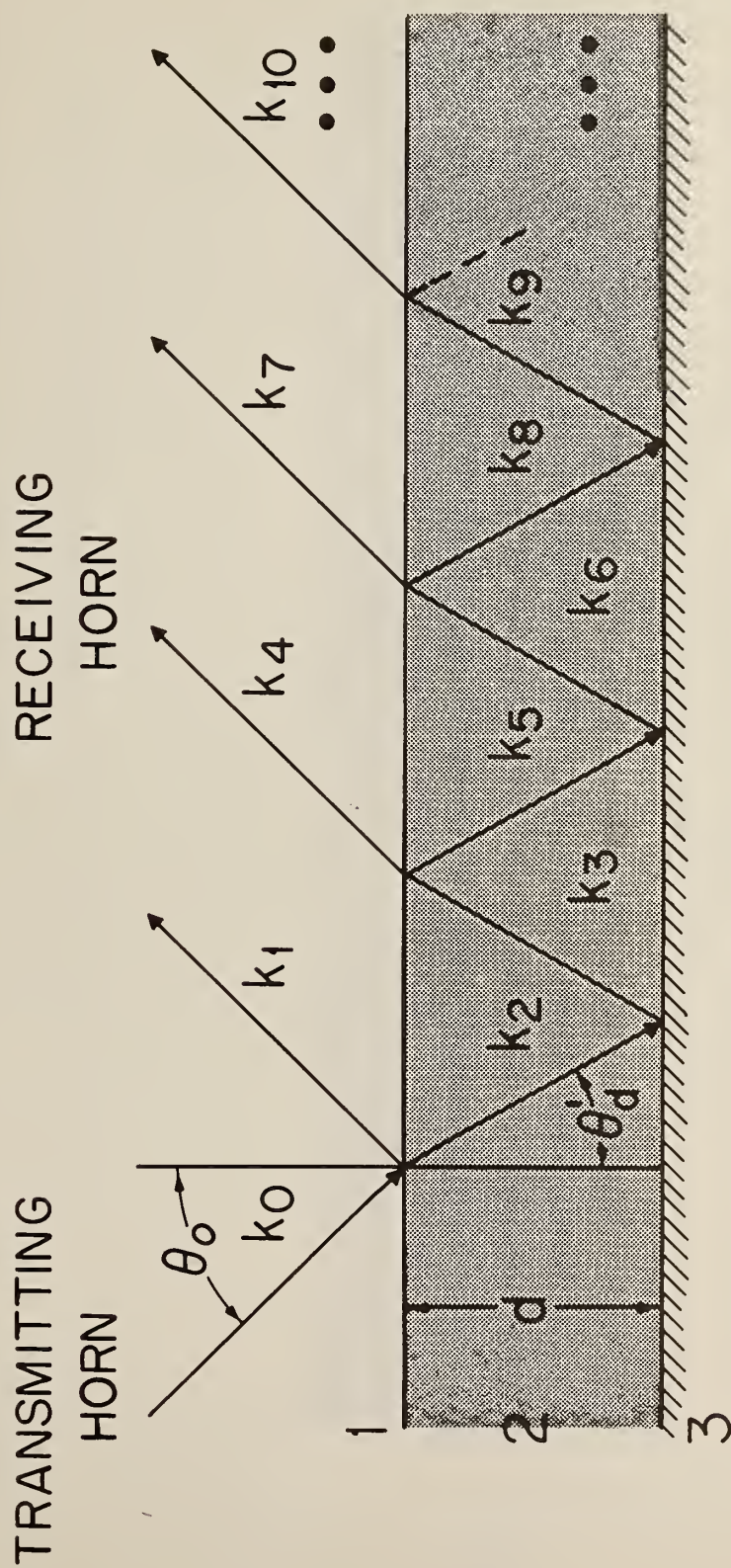
Figure 1: Multiple reflections of electromagnetic radiation in an air-dielectric-metal configuration for real angles of refraction θ'_d.
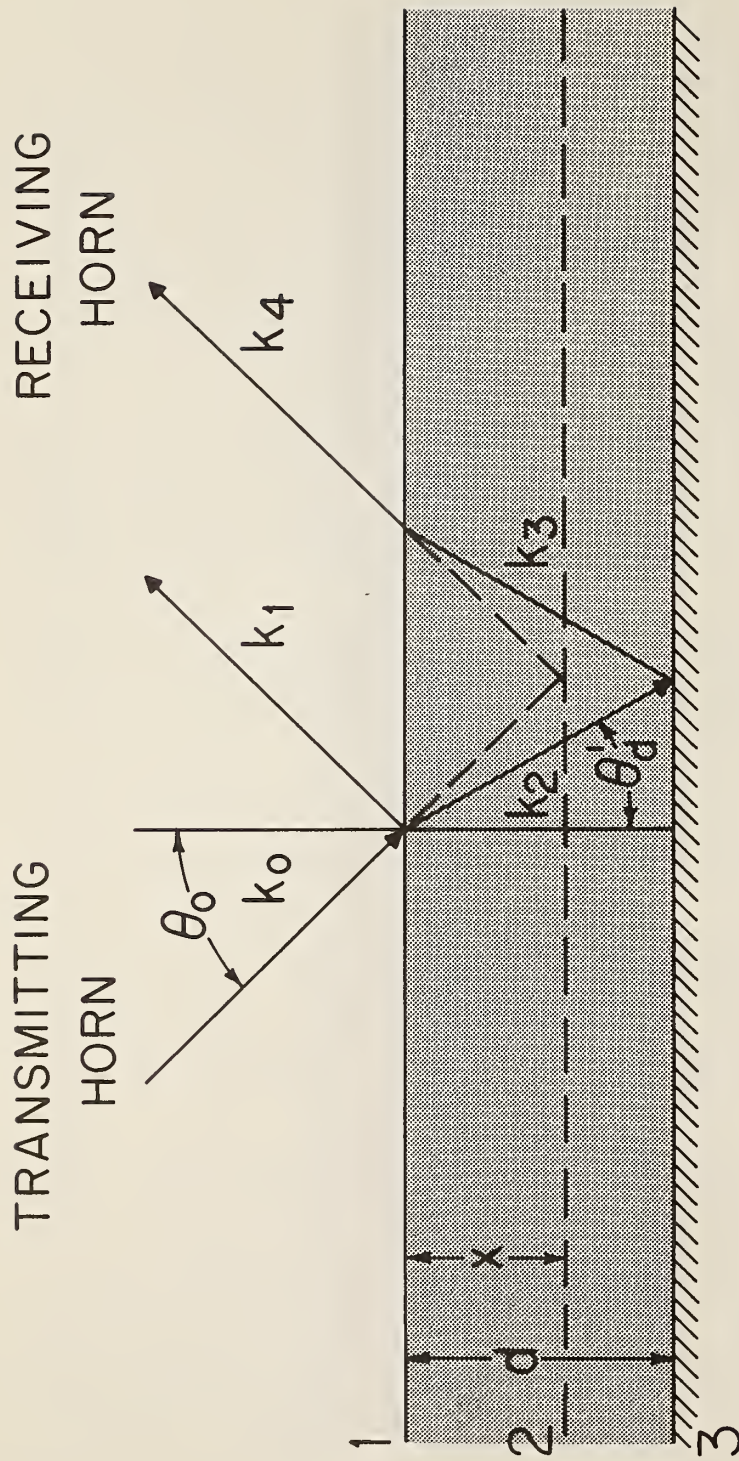
Figure 2: Geometrical model employed to define the variable x = x(d).

Interferometric Measurements of the Complex
Dielectric Constant of Liquids

IV. A Numerical Method for Determining the
Best Complex Dielectric Constant

Lynn M. Thiel

and

William S. Lovell

ABSTRACT

A numerical method is presented for determining the best
complex dielectric constant $\epsilon^* = \epsilon' - i\epsilon''$ from an experimental record
obtained at millimeter-wavelengths from free-space, interferometric
measurements of liquids. The method of selected points is applied to
the reflection coefficient expression to obtain a set of simultaneous
equations which is solved for an initial vector solution using the
generalized Newton iteration function. The principle of least squares
is then applied to achieve the best fit between the reflection coefficient
expression and experimental record. The desired values of ϵ' and ϵ''
are included as components of a final vector solution of the best fitting
theoretical curve.

1. INTRODUCTION

Previous methods for the determination of the complex dielectric constant $\epsilon^* \equiv \epsilon' - i\epsilon''$ of liquids utilizing free-space, interferometric measurement techniques at millimeter wavelengths have not given dependable results. In this series of papers, three steps have been taken to obtain ϵ^* more accurately: (1) Methods which require approximations to an equation assumed to describe experimental results have been abandoned.[1] (2) The theory of the interferometric measurement technique has been re-examined.[2] (3) Effects occurring in the experiment not described by the theory have been minimized.[3]

A method of finding the best value for ϵ^* is presented in this paper. The method consists of fitting a theoretical curve to experimental data. For radiation polarized perpendicular to the plane of incidence, the function[2] which gives the theoretical curve can be written as

$$\Gamma_o \int_o^\infty \int_{\theta_o - \frac{\pi}{2}}^{\theta_o + \frac{\pi}{2}} f(\theta, \lambda; d) \, w(\theta, \lambda) \, d\theta d\lambda - R = 0 \, , \tag{1}$$

where

$$f(\theta, \lambda; d) = \frac{\rho^2 + 2\sigma \rho \cos(2\beta d + \delta - \psi) e^{-2\alpha d} + \sigma^2 e^{-4\alpha d}}{1 + 2\sigma \rho \cos(2\beta d - \delta - \psi) e^{-2\alpha d} + \sigma^2 \rho^2 e^{-4\alpha d}} \tag{2}$$

and

$$w(\theta, \lambda) = \frac{\exp\left\{ \frac{-1}{2(1-\tau^2)} \left[\left(\frac{x}{\sigma_x}\right)^2 - 2\tau\left(\frac{x}{\sigma_x}\right)\left(\frac{y}{\sigma_y}\right) + \left(\frac{y}{\sigma_y}\right)^2 \right] \right\} x'(\theta) y'(\lambda)}{2\pi \sigma_x \sigma_y \sqrt{1-\tau^2}} \cdot \tag{3}$$

The functions x and y are taken to be

$$x(\theta) = \tan(\theta - \theta_o) \; ; \qquad \qquad y(\lambda) = \lambda_o \ln(\lambda \lambda_o^{-1}) \, . \tag{4}$$

66

From the Fresnel reflection coefficient, ρ^2 and δ are defined by

$$\rho^2 = \frac{(\beta_g - \beta)^2 + \alpha^2}{(\beta_g + \beta)^2 + \alpha^2} \; ; \qquad\qquad \delta = \tan^{-1} \frac{2\alpha\beta_g}{\beta_g^2 - (\alpha^2 + \beta^2)} \; ; \quad (5)$$

where

$$\alpha = \frac{\beta_o}{\sqrt{2}} \; \{ \, [\, (\epsilon' - \sin^2 \theta)^2 + \epsilon''^2]^{\frac{1}{2}} - (\epsilon' - \sin^2 \theta) \}^{\frac{1}{2}} \; ;$$

$$\beta = \frac{\beta_o}{\sqrt{2}} \; \{ \, [\, (\epsilon' - \sin^2 \theta)^2 + \epsilon''^2]^{\frac{1}{2}} + (\epsilon' - \sin^2 \theta) \}^{\frac{1}{2}} \; ; \qquad\qquad (6)$$

$$\beta_g = \beta_o \cos \theta$$

for $\beta_o = 2\pi/\lambda$. The actual dielectric thickness d is defined by

$$d = (1 - \kappa)d_a + d_o \; . \qquad\qquad (7)$$

The left side of Eq. (1) is a function of the variables d_a and R, and contains as parameters the elements of the set $\Omega \equiv \{ \, \epsilon' , \, \epsilon'' , \, d_o , \, \theta_o , \, \lambda_o , \, \sigma , \, \psi , \, \kappa , \, \sigma_x , \, \sigma_y , \, \tau , \, \Gamma_o \}$, all of which have been defined previously.[2,3]

Some of the parameters of Ω cannot be estimated accurately by direct observation and must be evaluated mathematically. For convenience, let there be M of these unknown parameters and consider them to be the components of an M-dimensional vector $\underset{\sim}{v}$. The solution of a set of equations containing $\underset{\sim}{v}$ is the vector solution $\underset{\sim}{\alpha}$, where the components of $\underset{\sim}{\alpha}$ are the values given to the M unknown parameters to achieve the best fit between the theoretical curve and the experimental data. The best fit is defined by using the principle of least squares.

Although a set of equations containing $\underset{\sim}{v}$ obtained by substitution of data into Eq. (1) cannot be solved explicitly, the set can be solved numerically. Iterative techniques which can determine a solution to

any desired number of significant figures by successive application of an iteration function are employed. Derivations of two such iteration functions followed by their applications and an estimate of the accuracy of $\underset{\sim}{\alpha}$ will be presented.

2. THE ITERATION FUNCTIONS

Consider the M-dimensional real Hilbert space E^M of the vectors $\underset{\sim}{v} = (v_1, \ldots, v_M)$ with the Euclidean norm

$$\| \underset{\sim}{v} \| = (\underset{\sim}{v} : \underset{\sim}{v}) = \left[\sum_{m=1}^{M} v_m^2 \right]^{\frac{1}{2}}. \tag{8}$$

The space E^M is also a complete metric space with the Euclidean norm serving as the metric. Define the operator $\underset{\sim}{\varphi}$ which maps a closed subset $S \subset E^M$ into itself to be a contraction mapping.[4] Then, by the Banach Fixed Point Theorem, there exists a unique fixed point $\underset{\sim}{\alpha} \in S$ such that

$$\underset{\sim}{\varphi}(\underset{\sim}{\alpha}) = \underset{\sim}{\alpha}. \tag{9}$$

The point $\underset{\sim}{\alpha}$ can be found from the recursion relation

$$\underset{\sim}{v}^{(k+1)} = \underset{\sim}{\varphi}(\underset{\sim}{v}^{(k)}) \tag{10}$$

for $\underset{\sim}{v}^{(0)} \in S$ by taking the limit to get

$$\underset{\sim}{\alpha} = \lim_{k \to \infty} \underset{\sim}{v}^{(k+1)} = \lim_{k \to \infty} \underset{\sim}{\varphi}(\underset{\sim}{v}^{(k)}). \tag{11}$$

The mapping $\underset{\sim}{\varphi}$ is classified as a one-point iteration function.[5]

For practical applications, what is meant by convergence of $\left\{ \underset{\sim}{v}^{(k)} \right\}$ and what constitutes a solution must be stated clearly. Since $\underset{\sim}{\alpha}$ is a limit point of $\left\{ \underset{\sim}{v}^{(k)} \right\}$ if and only if α_i is a limit point of $\left\{ v_i^{(k)} \right\}$ for $1 \leq i \leq M$, then by the Cauchy convergence principle, Eq. (11) holds if and only if, given any $\epsilon > 0$, there exists an integer $N_i(\epsilon)$ such that

$$\left| v_i^{(m)} - v_i^{(n)} \right| < \epsilon \tag{12}$$

whenever $m, n \geq N_i$ for $1 \leq i \leq M$. Let $N(\epsilon) \equiv \max_{1 \leq i \leq M} \left\{ N_i(\epsilon) \right\}$. Then Eq. (11) holds if and only if, given $\epsilon > 0$, the inequality (12) is satisfied whenever $m, n \geq N$ for $1 \leq i \leq M$. By similar reasoning, $\left\{ \underset{\sim}{v}^{(k)} \right\}$ is said to converge in practice if for a specified $\epsilon > 0$,

$$\left| v_i^{(k+1)} - v_i^{(k)} \right| < \epsilon \tag{13}$$

for all $1 \leq i \leq M$ and for the number of iterations $(k+1) \leq K(\epsilon)$, where K is some positive integer. The vector $\underset{\sim}{v}^{(k+1)}$ is then taken to be the desired solution $\underset{\sim}{\alpha}$.

Generalized Newton Iteration Function

Consider a system of nonlinear equations

$$F_m(\underset{\sim}{v}) = 0, \quad m = 1, \ldots, M \tag{14}$$

where $F_1, \ldots, F_m$ are real valued functions defined on E^M. If the function $\underset{\sim}{F}$ mapping E^M into itself is defined by $\underset{\sim}{F} = (F_1, \ldots, F_m)$, then Eqs. (14) can be written as

$$\underset{\sim}{F}(\underset{\sim}{v}) = \underset{\sim}{0}. \tag{15}$$

To find an explicit expression for $\underset{\sim}{\varphi}$ of Eq. (10) by inverse inter-polation[6], let each F_m have continuous first partial derivatives in some neighborhood of $\underset{\sim}{\alpha}$, $N(\underset{\sim}{\alpha})$, and assume that the Jacobian matrix

$$J(\underset{\sim}{v}) = [J_{ij}] = \left[\frac{\partial F_i}{\partial v_j} \right] \tag{16}$$

is nonsingular in $N(\underset{\sim}{\alpha})$. If $\underset{\sim}{G}$ is the functional inverse of $\underset{\sim}{F}$, then

$$\underset{\sim}{\alpha} = \underset{\sim}{G}(0). \tag{17}$$

Expand the right side of Eq. (17) in a Taylor's series about $\underset{\sim}{u} \in E^M$ to

get

$$\alpha_m = G_m(\underset{\sim}{u}) - \sum_{j=1}^{M} \frac{\partial G_m(\underset{\sim}{u})}{\partial u_j} u_j + \frac{1}{2} \sum_{i=1}^{M} \sum_{j=1}^{M} \frac{\partial^2 G_m(\underset{\sim}{u})}{\partial u_i \partial u_j} u_i u_j + \ldots, \quad (18)$$

for $1 \leq m \leq M$. Observe that

$$u_m = F_m(\underset{\sim}{v}) ; \qquad\qquad v_i = G_i(\underset{\sim}{u}) . \qquad\qquad (19)$$

From Eqs. (19),

$$du_m = \sum_{i=1}^{M} \frac{\partial F_m(\underset{\sim}{v})}{\partial v_i} dv_i ; \qquad dv_i = \sum_{j=1}^{M} \frac{\partial G_i(\underset{\sim}{u})}{\partial u_j} du_j . \qquad (20)$$

Substitution for dv_i into the first equation of (20) yields

$$du_m = \sum_{i=1}^{M} \sum_{j=1}^{M} \frac{\partial F_m(\underset{\sim}{v})}{\partial v_i} \frac{\partial G_i(\underset{\sim}{u})}{\partial u_j} du_j \qquad\qquad (21)$$

which implies

$$\sum_{i=1}^{M} \frac{\partial F_m(\underset{\sim}{v})}{\partial v_i} \frac{\partial G_i(\underset{\sim}{u})}{\partial u_j} = \sum_{i=1}^{M} J_{mi} \frac{\partial G_i(\underset{\sim}{u})}{\partial u_j} = \delta_{mj} \qquad (22)$$

where δ_{mj} is the Kronecker delta. If the elements of the inverse Jacobian matrix, J^{-1}, are denoted by J_{ij}^{-1}, then by Eq. (22)

$$\frac{\partial G_i(\underset{\sim}{u})}{\partial u_j} = J_{ij}^{-1} , \qquad\qquad (23)$$

since $J J^{-1} = I$, the $\underline{Mth}$ order identity matrix. Substitution of Eqs. (19) and (23) into (18) gives

$$\alpha_m = v_m - \sum_{j=1}^{M} J_{mj}^{-1} F_j(\underset{\sim}{v}) + O(\| \underset{\sim}{F}(\underset{\sim}{v}) \|^2) \qquad\qquad (24)$$

for $1 \leq m \leq M$, where the remainder $O(\| \underset{\sim}{F}(\underset{\sim}{v}) \|^2)$ is of order $\| \underset{\sim}{F}(\underset{\sim}{v}) \|^2$. Truncating the right side of Eqs. (24) to eliminate $O(\| \underset{\sim}{F}(\underset{\sim}{v}) \|^2)$ yields, using matrix notation, the iteration function

$$\underset{\sim}{\varphi}(\underset{\sim}{v}) = \underset{\sim}{v} - J^{-1}(\underset{\sim}{v}) \underset{\sim}{F}(\underset{\sim}{v}) , \qquad (25)$$

where $\underset{\sim}{\varphi}$, $\underset{\sim}{v}$, and $\underset{\sim}{F}$ can be considered as column vectors. This is the generalized Newton iteration function, GNIF, and has been shown to be of second order.[7]

Least Squares Iteration Function

To obtain $\underset{\sim}{\alpha}$ from an initial approximation $\underset{\sim}{v}^{o}$, consider a real valued function F of the form

$$F(x, y; \underset{\sim}{v}) = 0 \qquad (26)$$

which is to be fitted to the set of N observed points $P_o = \{(x_n^o, y_n^o) \mid n = 1, \ldots, N\}$. Each x_n^o or y_n^o is assumed to contain a random experimental error which is independent of the errors in all other coordinates of the points in P_o. Also, there exists a corresponding set of N adjusted or calculated points $P = \{(x_n, y_n) \mid n = 1, \ldots, N\}$. To each x_n^o and y_n^o there is associated a weight w_{x_n} and w_{y_n}, respectively, which is dependent on the confidence held in the accuracy of that coordinate. Define the residuals $X_n = x_n^o - x_n$, $Y_n = y_n^o - y_n$, and $V_m = v_m^o - v_m$ for $1 \leq n \leq N$ and $1 \leq m \leq M$. Since all $(x_n, y_n) \in P$ lie on the calculated curve described by Eq. (26),

$$F(x_n, y_n; \underset{\sim}{\alpha}) = \underset{\sim}{0}, \quad n = 1, \ldots, N \qquad (27)$$

which imposes N conditions on the elements in P. The principle of least squares requires that

$$S = \sum_{n=1}^{N} (w_{x_n} X_n^2 + w_{y_n} Y_n^2) \qquad (28)$$

be minimized with respect to the points in P restricted by the N

conditions imposed by Eqs. (27). The fit which yields the minimum value of S, S_{min}, is defined as the _best_ _fit_.

For each $(x_n^o, y_n^o) \in P_o$ and $\underset{\sim}{v}^o$, Eq. (26) in general is not satisfied. Let F_n^o be some number such that $F_n^o = F(x_n^o, y_n^o; \underset{\sim}{v}^o)$ for $1 \leq n \leq N$. The conditions of (27) are made linear in the residuals by expanding the left side of Eq. (26) in a Taylor's series about $(x_n, y_n; \underset{\sim}{\alpha})$. Neglecting higher-order terms and using Eqs. (27) gives the reduced conditions

$$F_n^o = F_x^n X_n + F_y^n Y_n + \sum_{m=1}^{M} F_{\alpha_m}^n V_m, \quad n=1, \dots, N \qquad (29)$$

where the notation F_t^n means partial derivative of F with respect to t, evaluated at $(x_n, y_n; \underset{\sim}{\alpha})$.

To find S_{min} subject to the constraints of Eqs. (27) or equivalently of Eqs. (29), the method of Lagrange multipliers[8] is used. For this let

$$g_n = [F_x^n X_n + F_y^n Y_n + \sum_{m=1}^{M} F_{\alpha_m}^n V_m] - F_n^o, \quad n = 1, \dots, N \qquad (30)$$

and consider S to be a function also of the V_m's with zero coefficients. Form the linear combination

$$\Phi = S + \sum_{n=1}^{N} \lambda_n g_n, \qquad (31)$$

where $\lambda_1, \dots, \lambda_N$ are arbitrary constants. A solution which minimizes S will also satisfy the system of equations

$$\frac{\partial \Phi}{\partial X_n} = 0, \qquad \frac{\partial \Phi}{\partial Y_n} = 0, \qquad \frac{\partial \Phi}{\partial V_m} = 0, \quad \begin{matrix} n=1, \dots, N \\ m=1, \dots, M \end{matrix} \qquad (32)$$

and

$$g_n = 0, \quad n = 1, \dots, N. \qquad (33)$$

Observe that Eqs. (32) reduce to

$$2w_{x_n} X_n + \lambda_n F_x^n = 0 \; , \qquad 2w_{y_n} Y_n + \lambda_n F_y^n = 0, \qquad n = 1, \dots, N \qquad (34)$$

and

$$\sum_{n=1}^{N} \lambda_n F_{\alpha_m}^n = 0 \; , \qquad m = 1, \dots, N \; , \qquad (35)$$

respectively. If the residuals in Eqs. (34) are solved to get

$$X_n = \frac{\Lambda_n F_x^n}{w_{x_n}} \; ; \qquad Y_n = \frac{\Lambda_n F_y^n}{w_{y_n}} \; , \qquad n = 1, \dots, N \qquad (36)$$

where $\Lambda_n = -\frac{1}{2} \lambda_n$, their values substituted into Eqs. (33), and the coefficients of the Λ_n's collected into the coefficients

$$L_n = \frac{(F_x^n)^2}{w_{x_n}} + \frac{(F_y^n)^2}{w_{y_n}} \; , \qquad n = 1, \dots, N, \qquad (37$$

then Eqs. (33) reduce to

$$F_o^n = L_n \Lambda_n + \sum_{m=1}^{M} F_{\alpha_m}^n V_m , \qquad n = 1, \dots, N \qquad (38)$$

which can be solved to give

$$\Lambda_n = \frac{1}{L_n} (F_o^n - \sum_{m=1}^{M} F_{\alpha_m}^n V_m), \qquad n = 1, \dots, N . \qquad (39)$$

Also, Eqs. (35) can be written as

$$\sum_{n=1}^{N} \Lambda_n F_{\alpha_m}^n = 0 \; , \qquad m = 1, \dots, M . \qquad (40)$$

Substitution of Eq. (39) into (40) yields after rearrangement

$$\sum_{j=1}^{M} \left[\sum_{n=1}^{N} \frac{F_{\alpha_m}^n \, F_{\alpha_j}^n}{L_n} \right] V_j = \sum_{n=1}^{N} \frac{F_o^n \, F_{\alpha_m}^n}{L_n} \, , \qquad m = 1, \ldots, M . \quad (41)$$

In matrix notation, Eqs. (41) can be written as $CV = B$, where the elements C_{mj} of the $M \times M$ symmetrical coefficient matrix, C, are given by the quantities inside the brackets on the left side of Eqs. (41), the elements B_m of the $M \times 1$ matrix B are given by the terms on the right side of Eqs. (41), and the elements of the $M \times 1$ matrix V are $V_1, \ldots, V_M$. If C is nonsingular, the residual vector V can be solved for as $V = C^{-1}B$, and the corrected approximate solution is

$$\underset{\sim}{v} = \underset{\sim}{v}^o - V = \underset{\sim}{v}^o - C^{-1}B , \quad (42)$$

where $\underset{\sim}{v}$ and $\underset{\sim}{v}^o$ can be considered to be column matrices. The least squares iteration function, LSIF, which depends on all of the points in P_o, can now be defined by

$$\varphi \, (\underset{\sim}{v}) = \underset{\sim}{v} - C^{-1}(\underset{\sim}{v}) \, B \, (\underset{\sim}{v}) . \quad (43)$$

The derivatives in Eq. (29) were evaluated at the point $(x_n, y_n; \underset{\sim}{\alpha})$. For most practical applications of φ defined in Eq. (43), it suffices instead to evaluate these derivatives at the available point $(x_n^o, y_n^o; \underset{\sim}{v}^o)$.

3. DETERMINATION OF THE VECTOR SOLUTION

The solution of Eqs. (14) or (26) is dependent on the experimental data. The data[2] consists of a sequence of power level readings, $\{ R_n \mid n = 1, \ldots, N \}$; observed initial estimates of the parameters in Ω; the total change in thickness, Δd, of the dielectric liquid; and the index of some extremum, either a maximum or a minimum, of an experimental record P_N. P_N constitutes the set P_o and is defined by $P_N = \{ (d_{a,n}, R_n) \mid n = 1, \ldots, N \}$, where the assumed thicknesses are given by

$$d_{a,1} = 0 ; \qquad d_{a,n} = d_{a,n-1} + \frac{\Delta d}{N-1} , \qquad n = 2, \ldots, N . \quad (44)$$

Assuming that Eq. (1) describes the experimental record for the proper values of the parameters in Ω, $\underset{\sim}{\alpha}$ can now be determined.

Analysis of the Integration

Evaluation of the function of Eq. (1) and its partial derivatives requires integration of a real valued function $g = g(\theta, \lambda; d_{a,n}; \underset{\sim}{v})$ over an area A in the θ, λ - plane, where $g \equiv \Gamma_o \, f \cdot w$ of Eq. (1). For obvious reasons the integration is performed numerically over an A of finite dimensions. The basis and technique required for this integration are now presented.

Numerical Integration for a Double Integral

Let f be a real valued integrable function defined on some connected region of E^2. An approximate integral over a rectangular area A is given by the formula[9]

$$\iint\limits_A f(x, y) \, dxdy \approx \sum_{i=1}^{n_1} \sum_{j=1}^{n_2} w_{ij} \, f(x_i, y_j) \tag{45}$$

where the w_{ij} are the weights determined by "squaring" an appropriate Lagrangian formula for integration with one variable[10]. For this, let L_1 and L_2 be $n_1 \times 1$ and $n_2 \times 1$ matrices, respectively, whose elements are the weights w_j^i, $i = 1, 2$ for the formulae

$$\int_{a_i}^{b_i} f_i(x) \, dx \approx \sum_{j=1}^{n_i} w_j^i \, f_i(x_j), \quad i = 1, 2 \ . \tag{46}$$

The matrix of weights w_{ij} are then given by the outer product of L_1 and L_2, i.e., by $L_1 \widetilde{L}_2 = [w_{ij}]$, where $w_{ij} = w_i^1 w_j^2$.

To apply Eq. (45), let $(b_1 - a_1) = h_1 \sigma_x$ and $(b_2 - a_2) = h_2 \sigma_y$, where h_1 and h_2 are sufficiently large so that $w(\theta, \lambda) \approx 0$ for $\theta \notin S_1 = [a_1, b_1]$ or $\lambda \notin S_2 = [a_2, b_2]$. This is possible since w defined

in Eq. (3) is a normal frequency function of x and y. Then A is defined by the Cartesian product $S_1 \times S_2$.

Differentiation Under the Integral Sign

The real valued function of Eq. (1) can be written as

$$F(d_{a,n}, R_n; \underset{\sim}{v}) = \iint\limits_{A} g(\theta, \lambda; d_{a,n}; \underset{\sim}{v}) \, d\theta d\lambda - R_n . \qquad (47)$$

Application of the GNIF and the LSIF requires evaluation of the partial derivatives $F_{d_{a,n}}$, F_{R_n}, and F_{v_m}. Except for F_{R_n}, differentiation of an integral expression is then necessary. Since the derivatives[11] are found analytically and the integration is performed numerically, it is desirable to have

$$\frac{\partial F}{\partial d_{a,n}} = \frac{\partial}{\partial d_{a,n}} \iint\limits_{A} g \, d\theta d\lambda = \iint\limits_{A} \frac{\partial g}{\partial d_{a,n}} \, d\theta d\lambda ;$$

$$\frac{\partial F}{\partial v_m} = \frac{\partial}{\partial v_m} \iint\limits_{A} g \, d\theta d\lambda = \iint\limits_{A} \frac{\partial g}{\partial v_m} \, d\theta d\lambda . \qquad (48)$$

If Eqs. (48) hold, then F and its partial derivatives can be obtained by numerical integration of g and its partial derivatives. If A is a compact subset of E^2, B an open set of E^{M+1}, and g, along with its partial derivatives, is continuous on the Cartesian product A × B = $\{ (\theta, \lambda; d_{a,n}; \underset{\sim}{v}) \mid (\theta, \lambda) \in A, (d_{a,n}; \underset{\sim}{v}) \in B \}$, then it has been proven[12] that Eqs. (48) hold and the partial derivatives are continuous.

Application of the Iteration Functions

Before applying the previous theory, it should be stated that all of the conditions that have been imposed on the function (47), its derivatives, parameters, and variables are satisfied. The assumptions that the Jacobian and coefficient matrices are nonsingular are valid if neither the set of Eqs. (14) nor (26) is functionally dependent.[13]

Functional dependence can be avoided by the proper choice of para-
meters to be included as components of $\underset{\sim}{v}$. With all of these
stipulations met, $\underset{\sim}{\alpha}$ is determined in the following three steps.

Initial or Given Parameters

All of the parameters of Ω are to be given initial values. Since
functional dependence is to be avoided, only M of those parameters
are included as components of $\underset{\sim}{v}$. The initial values given these M
parameters are only approximate and will be adjusted using the
GNIF and then the LSIF. The remaining parameters are treated as
known constants and their initial values are final.

To determine initial values for ϵ^* and d_o, consider a set of K
extrema, $\{ (R_{k_i}, d_{a,k_i}) \mid i = 1, \ldots, K\}$ and the corresponding array
of indices, $\{n_{k_i} \mid i = 1, \ldots, K\}$, where $n_k = \dfrac{k}{2}$ for $k = 1, 2, \ldots$. The
set of extrema can be determined to sufficient accuracy from the
experimental record using a scanning routine if $\Delta d/(N-1)$ is sufficiently
small. The corresponding values for the index array are then
obtained utilizing the index of the given extremum mentioned earlier.
An approximation[1,2] to Eq. (1) which assumes $\psi = \delta = \pi$,
$\lambda_d = 2(d_{a,k_j} - d_{a,k_i}) / (n_{k_j} - n_{k_i})$ for all $i \neq j$, and (θ, λ) not distributed
enables ρ to be solved for as

$$\rho = \frac{R_{k_i}^{\frac{1}{2}} - (-1)^{2n_{k_i}} \Gamma_o^{\frac{1}{2}} \sigma e^{-n_{k_i}\alpha\lambda_d}}{\Gamma_o^{\frac{1}{2}} - (-1)^{2n_{k_i}} R_{k_i}^{\frac{1}{2}} \sigma e^{-n_{k_i}\alpha\lambda_d}} \tag{49}$$

for $1 \leq i \leq K$. Eliminating ρ between any two equations of the form
(49) for $i \neq j$ yields the function f defined as

$$f(\alpha\lambda_d) = 1 + s_1\sigma^2 e^{-(n_{k_i} + n_{k_j})\alpha\lambda_d} + R_{ij}\left(e^{-n_{k_i}\alpha\lambda_d} + s_1 e^{-n_{k_j}\alpha\lambda_d}\right) = 0, \tag{50}$$

where

77

$$R_{ij} = s_2 \left(\frac{R_{k_i}^{\frac{1}{2}} R_{k_j}^{\frac{1}{2}} - \Gamma_o^{\frac{1}{2}}}{R_{k_i}^{\frac{1}{2}} - R_{k_j}^{\frac{1}{2}}} \right) \tag{51}$$

for $s_1 = \begin{cases} -1, \text{ extrema of the same type} \\ 1, \text{ otherwise} \end{cases}$ and $s_2 = \begin{cases} -1, \text{ extrema both min.} \\ 1, \text{ otherwise} \end{cases}$.

Equation (50) is solved numerically for $\alpha\lambda_d$, which requires an initial approximation $z^{(0)}$ to $z = \alpha\lambda_d$. $z^{(0)}$ is found by scanning the positive z-axis by increments of Δz, starting at some small $z_o > 0$ and letting

$$z^{(0)} = z_o + \frac{2p+1}{2} \Delta z \tag{52}$$

when $f(z_o + p\,\Delta z)\; f(z_o + (p+1)\,\Delta z) \le 0$ for some positive integer p. The root $\alpha\lambda_d$ is determined accurately using the recursively-formed iteration function[14]

$$\varphi(z) = \Psi_q(z) , \tag{53}$$

where

$$\Psi_1 = z ; \qquad \Psi_j(z) = \Psi_{j-1} - \frac{f(\Psi_{j-1}(z))}{f'(z)} , \quad j = 2, 3, \ldots, q . \tag{54}$$

The set of solutions obtained by considering various combinations of extrema is then processed for outliers[15] and the value for $\alpha\lambda_d$ is taken to be the average of the remaining solutions. The estimate for λ_d is given by

$$\lambda_d = \frac{2(1-\kappa)}{t} \sum_{i=1}^{t} \frac{d_{a,\,K-t+i} - d_{a,\,i}}{n_{K-t+i} - n_i} , \tag{55}$$

where t is the greatest integer of $\frac{1}{2}K$. The initial value for ϵ^* is now obtained from[1]

$$\epsilon' = \left(\frac{\lambda_o}{\lambda_d}\right)^2 \left[1 - \left(\frac{\alpha\lambda_d}{2\pi}\right)^2 \right] + \sin^2\theta ; \qquad \epsilon'' = \left(\frac{\lambda_o}{\lambda_d}\right)^2 \frac{\alpha\lambda_d}{\pi} . \tag{56}$$

78

The initial value for d_o is determined from the average of all

$$D_i = \frac{n_{k_i} \lambda_d}{2} - d_{a,k_i} \tag{57}$$

for $1 \leq i \leq K$, excluding those that are outliers.

The remaining initial values are established more directly. The initial values for θ_o, λ_o, κ, σ_x, and σ_y can be found experimentally. The initial value for σ lies between 0 and 1 and is estimated from previous experiments. The initial values for ψ and τ are close to π and 0, respectively. Finally, the initial value for Γ_o is taken to be somewhat greater than the power level reflected from a dry plate.[3] The initial values for θ_o, λ_o, σ, κ, and Γ_o so obtained are used in determining the initial values for ϵ^* and d_o.

Second Approximation to the Vector Solution

The method of selected points[16] is used to obtain a better approximation to $\underset{\sim}{\alpha}$ from the initial approximation. A set of M equations is defined by substituting M distinct points from P_N into Eq. (47) to get

$$F_m(\underset{\sim}{v}) = F(d_{a,n_m}, R_{n_m}; \underset{\sim}{v}), \quad m = 1, \ldots, M. \tag{58}$$

The inherent assumption here is that the points in P_N contain no experimental error and that for the proper choice of $\underset{\sim}{v}$, the theoretical curve passes through the M selected points. The solution of the set of equations (58) is found by applying the GNIF, using the initial values discussed previously.

Let $\{\underset{\sim}{\alpha}_j^o \mid j = 1, \ldots, N_M\}$ be the set of N_M second approximations to $\underset{\sim}{\alpha}$ found by considering N_M different sets of M points. The second approximation $\underset{\sim}{\alpha}^o$, which is most representative of the entire record, is then obtained in four steps: (1) All $\underset{\sim}{\alpha}_j^o$ for which their sequence of iterates did not converge to a point in E^M are eliminated from the set. (2) All $\underset{\sim}{\alpha}_j^o$ which converge outside some symmetric neighborhood of

the initial approximation to $\underset{\sim}{\alpha}$ are deleted from the set. (3) All $\underset{\sim}{\alpha}_j^o$ which constitute outliers are eliminated. The vector $\underset{\sim}{\alpha}_j^o$ is an outlier if any of its components are outliers with respect to the array of corresponding components of the set. (4) $\underset{\sim}{\alpha}^o$ is then taken to be the average of the remaining $\underset{\sim}{\alpha}_j^o$ in the set.

Final Vector Solution

The final solution $\underset{\sim}{\alpha}$ is the vector which yields the best fit between the theoretical curve and the experimental record. This vector is obtained from $\underset{\sim}{\alpha}^o$ by applying the LSIF. When the LSIF is used, every point of P_N contributes to the determination of $\underset{\sim}{\alpha}$.

For the present application of the LSIF, equal confidence is assumed in all coordinates of all points. Therefore, all weights can be set equal to one and then $\underset{\sim}{\alpha}$ is the vector which minimizes the sum of the squares of the residuals. This implies that all points of P_N contribute equally to the determination of $\underset{\sim}{\alpha}$.

4.   ACCURACY OF THE VECTOR SOLUTION

The utility of a determination of ϵ^* from an experimental record depends on the accuracy in the components of $\underset{\sim}{\alpha}$. If $\hat{\underset{\sim}{\alpha}}$ is the true vector estimated by $\underset{\sim}{\alpha}$, then the accuracy may be described in terms of the absolute error $\underset{\sim}{e} \equiv \underset{\sim}{\alpha} - \hat{\underset{\sim}{\alpha}}$. A measure of $\underset{\sim}{e}$ is given by

$$ \sigma_m = [\, (e_m)^2_{\text{mean}} \,]^{\frac{1}{2}} \,, \quad m = 1, \ldots, M \tag{59} $$

where the mean denotes the mean value of the square of the difference e_m. This is the average value that would be obtained if the vector solutions determined from experimental records repeated a large number of times under similar conditions were considered.

If the errors in the points of P_N are uncorrelated and these errors are small, it has been shown[17] that approximately unbiased estimates s_m^2 of σ_m^2 are given by

$$s_m^2 = \frac{S}{N-M} C_{mm}^{-1}, \quad m = 1, \ldots, M \tag{60}$$

where C_{ij}^{-1} is the i,jth element of the inverse of the coefficient matrix C^{-1}. The s_m are called the estimated standard errors of the components.

Once the s_m are determined, confidence intervals on the $\hat{\alpha}_m$ can be established.[18] If the probability of an event E occurring is P(E) where $0 \leq P(E) \leq 1$, p is a fixed percentage, and ζ_p is the p percent value of $\zeta = (\hat{\alpha}_m - \alpha_m)/s_m$ for the N-M degrees of freedom, then approximately

$$P(\alpha_m - \zeta_p s_m < \hat{\alpha}_m < \alpha_m + \zeta_p s_m) = 1 - \frac{p}{100} \tag{61}$$

for $1 \leq m \leq M$. The values ζ_p have been tabulated[19] for various p and degrees of freedom. Equations (61) say that there is the probability 100 - p% that the two random variables $\alpha_m \pm \zeta_p s_m$ will take on values which together include the unknown but true value $\hat{\alpha}_m$. Then the intervals $(\alpha_m - \zeta_p s_m, \alpha_m + \zeta_p s_m)$, $m = 1, \ldots, M$ are the 100 - p% confidence intervals for the α_m, the limits of the intervals are confidence limits for the α_m, and the corresponding confidence is 1 - p/100. Also there exists a 100 - p% chance that the magnitude of the absolute error in the mth component of α is smaller than $\zeta_p s_m$.

5. DISCUSSION

Although it is not possible to predict when a sequence of iterates obtained using one of the iteration functions previously discussed will converge, some observations are possible. Convergence will not occur if:

(1) One of the functions in Eqs. (14) or (26) or its partial derivatives becomes unbounded. In most cases the evaluated functions of Eqs. (14) or (26) must become small for convergence.

(2) The functions of Eqs. (14) or (26) are functionally dependent. Dependence can be caused by the inclusion in $\underset{\sim}{v}$ of parameters in Ω which are interdependent. For example, application of the above technique has shown that any subset of $\{\theta_o, \lambda_o, \sigma, \psi, \kappa\}$ consisting of three or more elements is interdependent. When functional dependence exists, the determinant of the Jacobian or coefficient matrix approaches zero and the norm of each iterate increases without bound.

(3) The vector $\underset{\sim}{v}$ contains a large number of components. Convergence is improved as the number of components of $\underset{\sim}{v}$ is decreased.

(4) A large neighborhood of $\underset{\sim}{\alpha}$ is necessary to include the initial approximation to $\underset{\sim}{\alpha}$. In general, the closer the initial approximation is to $\underset{\sim}{\alpha}$, the greater the probability for convergence. The vector composed of the inital values of the parameters described above is usually close enough to $\underset{\sim}{\alpha}$ to yield a number of convergences per record using the GNIF. The vector $\underset{\sim}{\alpha}^o$ is usually sufficient for convergence using the LSIF.

(5) The theory does not describe experimental conditions. This gives an important method of checking theoretical assertions, since the accuracy of the solution is dependent only upon the agreement between the theoretical description and the experimental record.

To evaluate ϵ^* in practice, the five parameters ϵ', ϵ'', d_o, σ, and Γ_o are usually included as components in $\underset{\sim}{v}$, hence their initial values are only approximate. However, there are other parameters which may be known only approximately that are not included in $\underset{\sim}{v}$. Errors in these parameters are absorbed by the values of some of the parameters in $\underset{\sim}{v}$. This compensation is possible because there exists interdependence between some parameters included in $\underset{\sim}{v}$ and

those not included. Since ϵ' and ϵ'' are observed not to be dependent on any other parameters, ϵ^* is unaffected by this compensation.

The second approximation to $\underset{\sim}{\alpha}$ using the GNIF is determined for two reasons. First, a number of $\underset{\sim}{\alpha}_j^o$ are attempted for each experimental record and the chance of obtaining at least a few convergences is good. Then since $\underset{\sim}{\alpha}^o$ is usually closer to $\underset{\sim}{\alpha}$ than the initial approximation, the probability of achieving convergence in subsequent use of the LSIF is increased. Secondly, convergence with the GNIF is, at least as empirically experienced in this application to the complex dielectric constant of liquids, much faster than with the LSIF. The reduction in the size of the neighborhood of $\underset{\sim}{\alpha}$ necessary to contain $\underset{\sim}{\alpha}^o$ substantially reduces the number of iterations performed in obtaining $\underset{\sim}{\alpha}$ using the LSIF.

If the partial derivatives of $g(\theta, \lambda; d_{a,n}; \underset{\sim}{v}^{(k)})$ are close to the partial derivatives of $g(\theta, \lambda; d_{a,n}; \underset{\sim}{v}^{(k+1)})$ the cost of computation per iteration using the LSIF can be decreased by not calculating new derivatives at each iteration. If new derivatives are not evaluated, then the coefficient matrix C remains the same and only the matrix B must be re-evaluated. Computation costs may also be reduced by not considering the distribution in (θ, λ) until the last iterations with the LSIF.

To demonstrate the relative agreement between the theoretical curve and the experimental record, consider the measure Δ defined by $\Delta(N; \underset{\sim}{\alpha}) = \dfrac{1}{N} \sum_{n=1}^{N} |F(d_{a,n}, R_n; \underset{\sim}{\alpha})|$, where F is defined in Eq. (47). Δ is the average difference in power level between the theoretical curve and the experimental record. The size of Δ depends on (1) the cardinality of P_N, (2) the size of the random error in the coordinates of each point in P_N, (3) the number of components of $\underset{\sim}{v}$, and (4) the agreement between theory and experiment.

Application of the techniques discussed in this paper necessitates use of a large digital computer.[20] The routine used here with Eq. (1)

83

was designed for more general application. In fact, any function satisfying the conditions imposed herein can be solved for a vector solution of any dimension using an arbitrary number of experimental points, providing also that the sequence of iterates converges.

APPENDIX: AN EFFICIENT MATRIX EVALUATION

Let P be an $M \times M$ nonsingular real matrix and Q be an $M \times 1$ real matrix. The evaluation of a matrix T of the form $T = P^{-1}Q$ is required for the practical application of Eqs. (14) and (26). An efficient computation of T is accomplished by forming the $M \times (2M+1)$ augmented matrix $[I, P, Q]$, where I is the $M \times M$ identity matrix, and then reducing the submatrix consisting of the last M columns to I by performing elementary row operations on the entire augmented matrix. The resultant matrix is $[T, P^{-1}, I]$, where T is the desired matrix. This procedure also yields the diagonal elements necessary for evaluating the estimated standard errors in Eq. (60). For details on the reduction of the augmented matrix see reference 21.

REFERENCES

1. W.S. Lovell, Paper I.

2. W.S. Lovell, L.M. Thiel, Paper III.

3. W.S. Lovell, Paper II.

4. I.P. Natanson, Theory of Functions of a Real Variable (Frederick Ungar Publishing Co., 1960) Vol. II, pp. 216-219.

5. J.F. Trabu, Iterative Methods for the Solution of Equations, Prentice-Hall, 1964) p.8.

6. Reference 5, pp.218-220.

7. Reference 5, p.221.

8. T.M. Apostol, Mathematical Analysis, (Addison-Wesley Publishing Co., Inc., 1957) pp.152-156.

9. M. Abramowitz and I.A. Stegun, Handbook of Mathematical Functions, (National Bureau of Standards, Applied Mathematics Series 55, Fifth Printing, August 1966, with corrections) p. 892.

10. R.A. Buckingham, Numerical Methods, (Pitman Publishing Co., 1957) pp.496-499.

11. A table of explicit derivatives is available upon request.

12. W.H. Fleming, Functions of Several Variables, (Addison-Wesley Publishing Co., Inc., 1965) pp.197-199.

13. P.F. Franklin, Methods of Advanced Calculus, (McGraw-Hill Book Co., Inc., 1944) pp.60-63.

14. Reference 5, pp.165-166.

15. W.J. Dixon, in A.E. Sarhan and B.G. Greenberg, Contributions to Order Statistics (John Wiley and Sons, Inc., 1962) Chap. 10H, pp.299-342.

16. W.E. Deming, Statistical Adjustment of Data, (John Wiley and Sons, Inc., 1948) p.52, 138.

17. J.R. Wolberg, Prediction Analysis, (D. Van Nostrand Co., Inc., 1967) pp.54-62.

18. H. Cramer, The Elements of Probability Theory, (John Wiley & Sons, Inc., 1955) pp.198-211.

19. Reference 18, p.274.

20. Listings of the Computer programs written in FORTRAN are available upon request.

21. J.B. Scarborough, Numerical Mathematical Analysis, (The John Hopkins Press, 1966) pp.284-297.

NBS TECHNICAL PUBLICATIONS

PERIODICALS

JOURNAL OF RESEARCH reports National Bureau of Standards research and development in physics, mathematics, chemistry, and engineering. Comprehensive scientific papers give complete details of the work, including laboratory data, experimental procedures, and theoretical and mathematical analyses. Illustrated with photographs, drawings, and charts.

Published in three sections, available separately:

● Physics and Chemistry

Papers of interest primarily to scientists working in these fields. This section covers a broad range of physical and chemical research, with major emphasis on standards of physical measurement, fundamental constants, and properties of matter. Issued six times a year. Annual subscription: Domestic, $5.00; foreign, $6.00*.

● Mathematical Sciences

Studies and compilations designed mainly for the mathematician and theoretical physicist. Topics in mathematical statistics, theory of experiment design, numerical analysis, theoretical physics and chemistry, logical design and programming of computers and computer systems. Short numerical tables. Issued quarterly. Annual subscription: Domestic, $2.25; foreign, $2.75*.

● Engineering and Instrumentation

Reporting results of interest chiefly to the engineer and the applied scientist. This section includes many of the new developments in instrumentation resulting from the Bureau's work in physical measurement, data processing, and development of test methods. It will also cover some of the work in acoustics, applied mechanics, building research, and cryogenic engineering. Issued quarterly. Annual subscription: Domestic, $2.75; foreign, $3.50*.

TECHNICAL NEWS BULLETIN

The best single source of information concerning the Bureau's research, developmental, cooperative and publication activities, this monthly publication is designed for the industry-oriented individual whose daily work involves intimate contact with science and technology—*for engineers, chemists, physicists, research managers, product-development managers, and company executives.* Annual subscription: Domestic, $1.50; foreign, $2.25*.

*Difference in price is due to extra cost of foreign mailing.

NONPERIODICALS

Applied Mathematics Series. Mathematical tables, manuals, and studies.

Building Science Series. Research results, test methods, and performance criteria of building materials, components, systems, and structures.

Handbooks. Recommended codes of engineering and industrial practice (including safety codes) developed in cooperation with interested industries, professional organizations, and regulatory bodies.

Special Publications. Proceedings of NBS conferences, bibliographies, annual reports, wall charts, pamphlets, etc.

Monographs. Major contributions to the technical literature on various subjects related to the Bureau's scientific and technical activities.

National Standard Reference Data Series. NSRDS provides quantitative data on the physical and chemical properties of materials, compiled from the world's literature and critically evaluated.

Product Standards. Provide requirements for sizes, types, quality and methods for testing various industrial products. These standards are developed cooperatively with interested Government and industry groups and provide the basis for common understanding of product characteristics for both buyers and sellers. Their use is voluntary.

Technical Notes. This series consists of communications and reports (covering both other agency and NBS-sponsored work) of limited or transitory interest.

CLEARINGHOUSE

The Clearinghouse for Federal Scientific and Technical Information, operated by NBS, supplies unclassified information related to Government-generated science and technology in defense, space, atomic energy, and other national programs. For further information on Clearinghouse services, write:

Clearinghouse
U.S. Department of Commerce
Springfield, Virginia 22151

Order NBS publications from:
Superintendent of Documents
Government Printing Office
Washington, D.C. 20402